# U.S. Economy and Global Stock Markets: Insights from a Distributional Approach

Ping Wu\* Dan Zhu<sup>†</sup> 24th November 2025

#### Abstract

Financial markets are interconnected, with micro-currents propagating across global markets and shaping economic trends. This paper moves beyond traditional stock market indices to examine cross-sectional return distributions—15 in our empirical application, each representing a distinct global market. To facilitate this analysis, we develop a matrix functional VAR method with *interpretable factors* extracted from cross-sectional return distrituions. Our approach extends the existing framework from modeling a single function to multiple functions, allowing for a richer representation of cross-sectional dependencies. By jointly modeling these distributions with U.S. macroeconomic indicators, we uncover the predictive power of financial market in forecasting macro-economic dynamics. Our findings reveal that U.S. contractionary monetary policy not only lowers global stock returns, as traditionally understood, but also dampens cross-sectional return kurtosis, highlighting an overlooked policy transmission. This framework enables conditional forecasting, equipping policymakers with a flexible tool to assess macro-financial linkages under different economic scenarios.

# 1 Introduction

Understanding macroeconomic and financial dependence involves recognizing how global stock markets are deeply connected to U.S. economic conditions. The stock market is a complex and multifaceted system, where myriad factors interact to influence asset prices and market dynamics. A growing body of macroeconomic literature focuses on constructing single financial indices as leading indicators for analyzing and predicting business cycles(Brunnermeier et al., 2021). Analyzing the market through broad indices can often oversimplify this intricate environment. At any given point in time, a stock market consists of a diverse pool of individual stocks, each exhibiting varying returns. This collection of returns from different stocks in the market forms a cross-sectional distribution, exhibiting the dispersion, skewness, and kurtosis of stock performance within the market. Analyzing this distribution provides deeper insights into market dynamics beyond aggregate indices, revealing how different segments of the market respond to economic conditions and policy changes.

One method to capture these variations is by graphing the density functions. As shown in the upper left panel of Figure 1, the S&P 500 in September 2008 and December 2018 experienced nearly identical overall index returns. However, the corresponding density plots, constructed using kernel estimation of constituent

<sup>\*</sup>ping.wu@strath.ac.uk University of Strathclyde

<sup>†</sup>dan.zhu@monash.edu Monash University

returns, reveal striking differences. In September 2008, the density plot displays fat tails, while in December 2018, it appears more normally distributed. A similar pattern is observed in China's market (upper right panel), where September 2008 and October 1999 share the same index level but exhibit completely different cross-sectional return distributions. These distinct features of cross-sectional distributions during crises—despite identical index levels to non-crisis periods—suggest a deeper interconnection with macroeconomic dynamics. In the literature, Kelly and Jiang (2014) extracted the time-varying tail index of returns from S&P 500 constituents, demonstrating its negative predictive power for real economic activity. Yet, focusing solely on how the U.S. stock market moves with macroeconomic variables is inadequate, especially amid trade wars and global political uncertainty. Poon et al. (2004) argue that the most efficient and effective way to study extreme events is through a multivariate approach, that the U.S. market has the greatest influence on other stock markets and one could expect that global financial market distributions tend to move together (as shown in the lower panel of Figure 1 about 15 international indices).

In this paper, we study 15 stock markets worldwide and analyse the dynamic evolution of the cross-sectional distribution of stock returns. This distributional perspective provides a more granular view of market behaviour, capturing shifts that aggregate indices may overlook. To summarise these distributions, we employ two complementary methods that transform the histograms in Figure 1 into a set of factors for each market at each point in time. The first method fits a skew-t distribution Azzalini and Capitanio (2003) to the empirical returns, yielding four parameters, location, scale, skewness, and degrees of freedom, for each of the 15 markets, and hence 60 factors in total. The second method approximates the log empirical distribution function using an orthonormal Fourier basis Crain (1974), with cosine functions capturing symmetric variation and sine functions capturing asymmetric variation. To ensure comparability across markets, we use a common basis globally and apply a matrix-variate factor model Wang et al. (2019) to obtain a parsimonious representation of distributional dynamics. We then combine these factors with key U.S. macroeconomic indicators in a Vector Autoregression (VAR) to trace how monetary policy shocks and macroeconomic fluctuations propagate through global financial systems.

Our framework expands the functional VAR literature Diebold et al. (2006) by jointly modelling multiple time-varying functions and macroeconomic variables within a unified system. Whereas traditional functional VARs typically analyse a single evolving function or treat several functions independently (Chang et al. (2024), we introduce 15 cross-sectional return distributions simultaneously, enabling a richer characterisation of global market dynamics. Both of our approaches extract interpretable, distribution-shaped factors that summarise key features of the cross-section, thereby providing a transparent link between cross-sectional return dynamics and macroeconomic conditions. The skew-t specification yields a fixed and economically interpretable set of parameters for each market, though dimensionality grows linearly as more markets are included. In contrast, the Fourier-based method produces equally meaningful distributional factors but, when combined with a matrix-variate factor model, achieves substantial dimensionality reduction. This leads to a scalable framework suited for large financial panels and other high-dimensional functional time-series applications. Taken together, these innovations allow us to capture global distributional dynamics in a computationally efficient and conceptually unified manner.

We evaluate the forecasting performance of the proposed approaches by comparing them with models that use standard global market factors. Our findings show that incorporating cross-sectional distributional information from global financial markets—whether through the skew-t parameters or the orthonormal basis coefficients—significantly improves the performance of the modeling in forecasting for macroeconomic indicators, compared to using a single index from each market. In particular, the functional approach

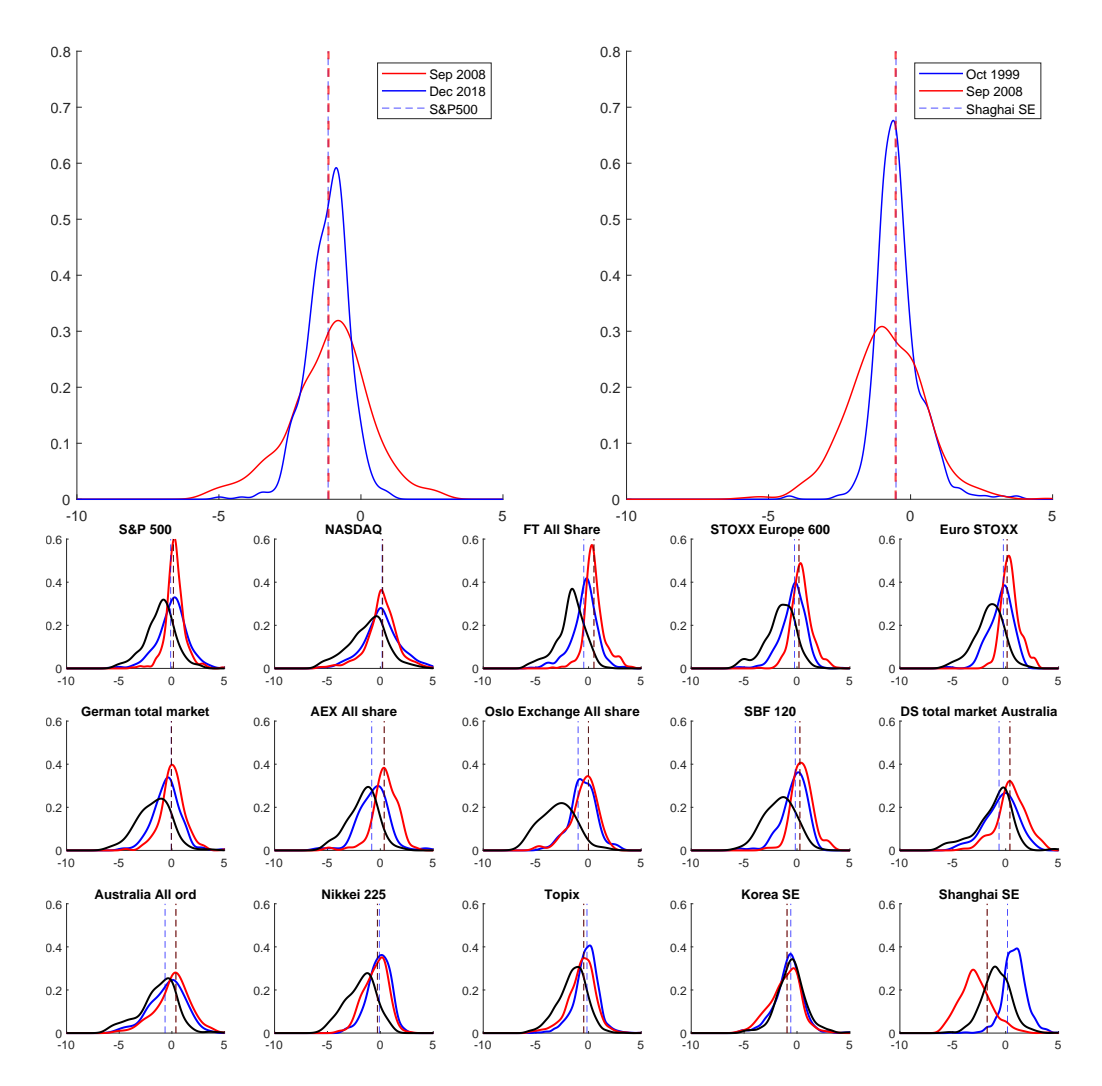


Figure 1: Hidden Heterogeneity: Index return and empirical return distributions (cross-sectional density constructed from constitutes' monthly price changes using kernel estimation). Upper panel: Two months with nearly identical returns on the overall S&P 500 and Shanghai SE index, yet with different empirical return distributions. Lower panel: Three months right before and the Global financial crisis. Blue: July 2008. Red: August 2008. Black: September 2008. Vertical lines: index return.

outperforms the skew-t specification by more effectively capturing complex distributional features, such as multimodality, which is a crucial characteristic of stock returns (Han, 2022) that the unimodal skew-t distribution cannot adequately represent.

After assuring the out-of-sample performance, we move forward to the structural analysis. Following (Bjørnland and Leitemo, 2009), we identify the structural VAR via long term restrictions. The findings on the mean response of global financial markets align with previous results, showing a negative shift in stock markets worldwide, with the Shanghai Stock Exchange being the exception. Additionally, we document a significant reduction in kurtosis across global stock markets following both expansionary and contractionary U.S. monetary policy shock, indicating a decline in the frequency of extreme market movements. Notably, this insight is only feasible through our specification, which integrates the entire distribution of stock market returns into the model rather than relying solely on aggregate indices. We conduct a conditional forecast exercise (Chan et al., 2024) assuming that the current market reaction will persist until July 2025. The

results suggest a prolonged period of elevated industrial production, leading to inflationary pressures and necessitating a higher federal funds rate. Additionally, global stock returns are expected to rise in response to the optimism surrounding Trump's victory.

The findings in the paper suggest key investment and macroeconomic policy implications. The documented reduction in kurtosis following U.S. monetary policy shock indicates a decline in extreme market movements, supporting investment strategies that reduce exposure to tail risks, such as volatilityselling or systematic option-writing approaches. Additionally, the anticipated rise in industrial production and inflationary pressures implies that inflation-sensitive assets—such as commodities, energy stocks, and value-oriented equities—may outperform, while higher interest rates could put downward pressure on longduration bonds, making short-duration fixed income or floating-rate instruments more attractive. The expected steepening of the yield curve presents opportunities in financial stocks, particularly banks, which benefit from improved net interest margins. Furthermore, the positive global equity outlook linked to optimism surrounding Trump's victory suggests an overweight stance on U.S. equities, with potential sector shifts favoring industries poised to benefit from expected pro-business policies. The Shanghai Stock Exchange's resilience to contractionary monetary spillovers highlights diversification opportunities in select Chinese equities, particularly in markets less exposed to global monetary tightening. From a policy perspective, these findings emphasize the role of monetary policy in shaping market risk and return distributions, underscoring the importance of incorporating distributional information in macro-financial forecasting and risk management. Policymakers should consider how monetary actions not only affect market levels but also alter cross-sectional dynamics, influencing investor sentiment, capital flows, and global financial stability.

The remainder of the paper is organized as follows. Section 2 discusses the data and methodology, detailing the proposed approaches for extracting distributional features from global stock markets and linking them to U.S. macroeconomic conditions. Section 3 examines the distributional responses of global stock markets to a U.S. monetary policy shock, shedding light on how such shocks propagate across markets. Section 4 presents conditional forecasts, under the scenario of Donald Trump's election success leading to US stock market surge. Finally, the appendix includes an out-of-sample forecasting horserace and provides additional results to support the main findings.

## 2 Data and Econometric Methods

To setup the context, we consider M financial markets,  $m \in \{1, ..., M\}$ . At each point in time for each market,  $f_{m,t}$  denote the cross-sectional distribution of returns such that  $\{y_{imt}\}_{i=1}^{N_m}$  are independent identically distributed draws from these distributions with  $N_m$  denote the number of stocks listed in market m. Assume that the support of these distributions are  $\mathbb{R}$ , we propose two methods to extract the distributional features,  $s_{m,t} \in \mathcal{S} \subset \mathbb{R}^s$  that

$$f_{m,t}(y) = f(y; s_{m,t}), y \in \mathbb{R}$$

where that simplifies the infinite dimensional problem of the distribution into a small set of parameters. We shall call these parameters, spanning factors, as they are time-varying.

Note that this i.i.d. assumption is not as restrictive as it may seem. At each market and time period, the returns from each company may follow its own distribution, i.e.,

$$Y_{imt} \mid \alpha_i, s_{m,t} \sim f(\cdot \mid \alpha_i, s_{m,t}).$$

Because company may not be observed consistently over time in each market, i.e., the S&P constituents may vary over time, we are not interested in estimating the individual  $\alpha_i$ 's. Instead, we can observe

$$Y_{imt} \mid s_{m,t} \sim f(\cdot \mid s_{m,t}) = \int f(\cdot \mid \alpha, s_{m,t}) d\pi(\alpha),$$

where the marginal distribution integrates out the company-specific effect  $\alpha$  according to the mixing distribution  $\pi(\alpha)$ .

A naive construction is to assume that returns are Gaussian, in which case the distribution is summarized by its mean and variance. However, such a moment-based characterization is often inadequate for financial markets, where return distributions typically exhibit skewness, heavy tails, volatility clustering, and other departures from normality. In addition, financial markets are segmented across industries, geographies, and market capitalizations, giving rise to heterogeneous and granular features in the cross-sectional distributions. Stocks within a market differ in size, sector, and exposure to global economic forces, and these differences are directly reflected in the distribution of returns. Market indices, such as the S&P 500, represent a special case of this framework, as they focus only on the central tendency of the distribution while ignoring higher-order features. To capture the richer structure of return distributions, we propose two complementary approaches: the first fits a skew-t distribution, and the second relies on a set of orthonormal basis functions under an exponential family structure. Both methods are then applied to analyze the dependence between global stock market returns and U.S. macroeconomic variables.

Given a finite set of factors  $\mathbf{S}_t$  extracted from the financial markets, we propose a VAR framework to jointly model the distributions of returns and macroeconomic variables,  $z_t \in \mathbb{R}^d$ . The VAR process has a simple formulation and is powerful to capture both contemporaneous and dynamic dependencies. Specifically, we define a  $X_t = \left[vec\left(\mathbf{S}_t\right)', z_t'\right]'$  as

$$X_{t} = b + \sum_{p=1}^{P} B_{p} X_{t-p} + \epsilon_{t}, \epsilon_{t} \sim N\left(\mathbf{0}_{dim}, \Sigma\right).$$

$$\tag{1}$$

#### 2.1 Data

The empirical analysis requires data that reflects global stock markets and U.S. economic conditions. We therefore consider the following two datasets covering the period from January 1995 to April 2025 (1995:01-2025:04).

The first dataset comprises 15 stock indices worldwide, covering the U.S., the U.K., Europe, Japan, South Korea, China, and Australia. All data series are on a monthly basis, using the last transaction date within each month. All are sourced from Datastream. The U.S. macroeconomy is represented through four key indicators: industrial production index (IP), consumer price index (CPI), trade balance (TB), and the federal funds rate (FFR). This selection is motivated by Flannery and Protopapadakis (2002), where they find nominal variables (e.g. CPI) are strongly correlated with stock market returns. All macro series are available from the FRED-MD database. The complete list of variables and how they are transformed are given in Appendix B.

#### 2.2 Skew-t Distribution

The first method involves skew-t distributions. The skew-t distribution is a versatile statistical model that extends the standard t-distribution by incorporating a skewness parameter, allowing it to capture evidently

asymmetric features in stock return data(Chang et al., 2013). It is characterized by four parameters: location, scale, skewness, and degrees of freedom, which together provide the flexibility to model both heavy tails and skewed distributions. This adaptability makes the skew-t distribution particularly useful in financial applications, where return distributions often exhibit asymmetry and tail behavior that deviate from normality.

In particular, we fit each  $f_{m,t}$  using a skew-t density function of Azzalini and Capitanio (2003)

$$f_{m,t}(y) = \frac{2}{\sigma_{m,t}} t_{\nu_{m,t}} \left( \frac{y - \mu_{m,t}}{\sigma_{m,t}} \right) T_{v_{m,t}+1} \left( \frac{\lambda_{m,t} \sqrt{1 + \nu_{m,t}} \left( \frac{y - \mu_{m,t}}{\sigma_{m,t}} \right)}{\left( \frac{y - \mu_{m,t}}{\sigma_{m,t}} \right)^2 + \nu_{m,t}} \right)$$

where  $t_v$  and  $T_v$  denote the probability density and cumulative density function of student t distribution with  $\nu$  degree of freedom. The four parameters  $s_{m,t} = (\mu_{m,t}, \sigma_{m,t}, \lambda_{m,t}, \nu_{m,t})'$  are obtained using maximum likelihood estimation.

Due to the high dimensions, we use the asymmetric conjugate prior of Chan (2022). An important advantage of this prior is that the conjugacy means analytical posterior results are available, thus reducing the computational burden. We call this model sktVAR.<sup>1</sup> In this analysis, we concentrate on the homoskedastic VAR framework, where the assumption of constant variance over time simplifies the model. For our purpose of understanding macroeconomic dependence within the stock market distribution, this homoskedastic approach captures the essential relationships and dynamics we are interested in, without the need to introduce additional complexity. While adding stochastic volatility could provide more detailed insights into time-varying uncertainty, incorporating it is not technically difficult and can be done without significantly altering the core structure of the model.

#### 2.3 Matrix Variate functional data

While the skew-t distribution is highly flexible, it is inherently unimodal and therefore unable to represent multimodal return distributions, as illustrated in Figure 1. In practice, multimodality frequently arises in financial markets as a result of segmentation, where different groups of assets—distinguished by sector, geography, or firm size—respond in distinct ways to macroeconomic shocks. These features are not static: during periods of market stress or regime shifts, the relative importance of different segments changes, and the cross-sectional distribution can evolve from unimodal to multimodal and back again. Menzly and Ozbas (2010) provide empirical evidence that such segmentation induces clustering in cross-sectional returns, highlighting the limitations of a unimodal framework and the need for methods that can accommodate dynamically changing multimodal structures.

Moreover, empirical analysis across 15 global financial markets reveals that our procedure extracts 60 distributional factors. Despite the seemingly large number, these factors exhibit a clear low-dimensional structure, with most of the variation concentrated in only a few dominant components, as shown in the scree plots in Appendix. This finding suggests that the complex cross-market dynamics of returns can, in fact, be summarized by a relatively small set of common drivers, providing both parsimony and interpretability in our representation.

<sup>&</sup>lt;sup>1</sup>In our application, M=15 is the number of stock markets, and d=4 is the number of macro variables, thus we have 64 dimension in the VAR. The prior is a version of the familiar Minnesota prior and the prior hyperparameters are set to be as comparable as possible across models. More specifically, the prior involves three hyperparameters as defined in Chan (2022).  $\kappa_1$  controls the overall shrinkage strength for coefficients on own lags, while  $\kappa_2$  controls those on lags of other variables. We set  $\kappa_1 = 0.01$  and  $\kappa_2 = 0.001$ . The remaining hyperparameter  $\kappa_3$ , which controls the shrinkage for the intercept, is set to 10.

We set up a joint modelling strategy, that is

$$\log f_{m,t}(y) = \Phi(y)' \mathbf{Z}_t \beta_m - \log \left( \int \exp\left(\Phi(x)' \mathbf{Z}_t \beta_m\right) dx \right)$$
 (2)

where  $\beta_m \in \mathbb{R}^{r_2}$  denote a vector of market specific coefficients and

$$\Phi(y) = [\phi_1(y), \phi_2(y), ..., \phi_{r_1}(y)]'$$

denote a vector of basis function that

$$\int \phi_j^2(y)dy = 1, \quad \int \phi_j(y)\phi_{j'}(y)dy = 0 \quad \text{for } j \neq j'$$

common across market spanning the functional space. Note here, we have  $s_{m,t} = \mathbf{Z}_t \beta_m$ , indicating that a low-dimensional common factor drives the distributional features across various markets. This specification is directly linked to the exponential family of distributions. In particular, the basis functions  $\Phi(y)$  play the role of sufficient statistics, while the coefficients  $\mathbf{Z}_t \beta_m$  act as the corresponding natural parameters. The normalizing integral ensures that the density integrates to one, analogous to the log-partition function in the exponential family. Thus, our framework can be viewed as an exponential family approximation to cross-sectional return distributions, where  $\Phi(y)$  provides a flexible yet structured set of sufficient statistics common across markets.

This specification is highly flexible, as the orthonormal basis expansion can approximate a wide range of distributional shapes, including multimodal structures that arise under market segmentation or regime shifts. Moreover, since the coefficients evolve with the common factors  $\mathbf{Z}_t$ , the framework naturally accommodates time-varying and dynamic changes in the cross-sectional return distributions across global markets.<sup>2</sup>

#### 2.3.1 An Iterative Algorithm

We implement an iterative procedure to estimate both the common factors and the market-specific coefficients, ensuring a robust decomposition of the cross-sectional return distributions. In each iteration, we first estimate the common factors by holding the market-specific coefficients fixed, leveraging the shared structure across markets to extract a low-dimensional representation of the underlying distributional dynamics. Next, we update the market-specific coefficients, conditioning on the estimated common factors, allowing each market's return distribution to retain its unique characteristics while maintaining a coherent global structure. In particular, we consider the following loglikelihood function

$$\mathcal{L}(\beta, Z) = \sum_{t=1}^{T} \sum_{m=1}^{M} \left( \left( \sum_{j=1}^{N_m} \Phi(y_{imt})' \mathbf{Z}_t \beta_m \right) - N_m \log \left( \int \exp\left(\Phi(x)' \mathbf{Z}_t \beta_m\right) dx \right) \right) - \frac{\gamma}{2} \sum_{m=1}^{M} \beta_m' \beta_m$$

and

<sup>&</sup>lt;sup>2</sup>Note that  $\mathbf{Z}_t$  and  $\boldsymbol{\beta}' = [\beta_1, ..., \beta_M]$  are still left unidentified, as an invertible matrix U amounts to  $Z_tU$  and  $U^{-1}\boldsymbol{\beta}'$  observational equivalent. A straightforward identification scheme is to set the top  $r_2 \times r_2$  block as a lower triangular matrix, i.e., in a similar fashion as the standard factor model identification scheme in Bai and Wang (2015).

1. Given  $\beta_1, ..., \beta_m$ , for t = 1, ..., T

$$\mathbf{Z}_{t} = \arg\max_{Z} \sum_{m=1}^{M} \left( \left( \sum_{j=1}^{N_{m}} \Phi(y_{jmt})' Z \beta_{m} \right) - N_{m} \log \left( \int \exp\left(\Phi(x)' Z \beta_{m}\right) dx \right) \right)$$

2. Given  $\mathbf{Z}_1, ..., \mathbf{Z}_T$ , for  $m = r_2 + 1, ..., M$ 

$$\beta_m = \arg\max_{\beta} \sum_{t=1}^{T} \left( \left( \sum_{j=1}^{N_m} \Phi(y_{jmt})' \mathbf{Z}_t \beta \right) - N_m \log \left( \int \exp\left( \Phi(x)' \mathbf{Z}_t \beta \right) dx \right) \right) - \frac{\gamma}{2} \beta_m' \beta_m$$

The alternating–maximization (update Z then  $\beta$ ) yields monotone ascent and converges to a block-stationary point shown in the Appendix. Because our model is in the exponential-family form with  $\Phi$  as sufficient statistics, the natural parameter for each cell (m,t) can be estimated independently from the data in that cell by solving the usual moment-matching (or single-cell MLE) problem; denote this estimate by  $s_{m,t}$ . Stacking these cellwise estimates across markets at a fixed time produces a matrix that, in population, factorizes into a time-specific factor  $Z_t$  and a market-loading matrix  $\beta$ , that  $Z_t$  and  $\beta$  can be recovered from the matrix of  $\{s_{m,t}\}$  by a simple (weighted) least-squares factorization. Practically, one can use these cellwise estimates either as a consistent initialization for the alternating likelihood algorithm or interleave them with the block updates; as cell sizes grow, the plug-in factorization is consistent, and the same rank/coverage conditions that ensure positive definiteness in our analysis guarantee stable recovery. Note that, while cellwise natural-parameter estimates are consistent as  $N_{m,t} \to \infty$ , in practice some markets/times have few returns, making  $s_{m,t}$  noisy or even ill-posed. The iterative likelihood algorithm remains crucial because it pools information across markets and times through  $(Z_t, \beta)$ , enforces identification/regularization, and thereby stabilizes and improves efficiency when  $N_{m,t}$  is small.

Note that there is a subtle difference between our specification and that of Chang et al. (2024): while they treat the macro variables and cross-sectional elements as part of the measurement equation, the density function is considered unobserved. Their more sophisticated approach implies that the measurement equation for the cross-sectional stock observations is nonlinear. In their paper, they linearize these equations to avoid the complexities of a nonlinear filter. Implementation of their approach is possible in our case, yet rather complicated, as it involves a multidimensional distribution where the sieve coefficients are cross-market dependent. Thus, we take the alternative route of treating the density as observed. To jointly model with macro variables,  $z_t$ , we specify  $X_t = \left[vec(\mathbf{Z}_t)', z_t'\right]'$  as a VAR process defined in Equation (1) with  $dim = (r_1r_2 + d)$ . We call this model mvfVAR.

#### 2.3.2 Functional Basis Properties: A Simulation Study

The choice of orthonormal basis functions is crucial for efficiently capturing salient distributional features. Although many alternatives exist, such as Legendre polynomials, we adopt a Fourier basis because it yields factors with clear and stable interpretations. Cosine functions span the symmetric component of the distribution, while sine functions span the asymmetric component, providing an immediate economic meaning to the extracted factors. Because the Fourier representation is a complete series expansion, this symmetric-asymmetric decomposition carries through all higher-order terms: lower frequencies capture broad features such as dispersion and skewness, whereas higher frequencies capture progressively finer symmetric or asymmetric deviations. A simulation study further illustrates this property, showing that

cosine coefficients predominantly capture symmetric variation (e.g., volatility), while sine coefficients capture asymmetric behaviour (e.g., skewness), resulting in an interpretable and structured representation of cross-sectional return distributions.

We design two data-generating processes (DGPs) to isolate these effects. The first DGP exhibits purely symmetric time-varying volatility:

$$r_t \sim \mathcal{N}(0, \sigma_t^2),$$
 (3)  
 $\sigma_t = 1 + 0.5 \cdot \sin\left(2\pi \frac{t}{200}\right).$ 

This process exhibits time-varying volatility but remains symmetric around zero at every point in time.

The second DGP incorporates both time-varying volatility and skewness using the Azzalini skew-t distribution:

$$r_t \sim \text{Skew-}t(\nu = 5, \lambda_t),$$

$$\sigma_t = 1 + 0.5 \cdot \sin\left(2\pi \frac{t}{300}\right),$$

$$\lambda_t = 0.5 \cdot \sin\left(2\pi \frac{t}{100}\right).$$

$$(4)$$

Our parameter choices reflect empirically relevant ranges for monthly financial returns. The volatility parameter  $\sigma_t$  varies between 0.5 and 1.5, corresponding to annualized volatilities of approximately 1.7% to 5.2%, which spans typical to moderately elevated market conditions. The skewness parameter  $\lambda_t$  varies between -0.5 and 0.5, generating conditional skewness in the range [-0.45, 0.45], consistent with empirical estimates for monthly equity returns. The degrees of freedom  $\nu = 5$  produces excess kurtosis, capturing the heavy-tailed characteristics commonly observed in financial data. The different periodicities for volatility (period=300) and skewness (period=100) allow us to distinguish their respective effects on the basis coefficients.

We use deterministic processes rather than stochastic ones (e.g., random walk volatility) to provide clear, identifiable signals for demonstrating the mapping between economic features and basis functions. This controlled setting allows us to cleanly isolate the roles of sine and cosine components without the confounding effects of more complex dynamics. While empirical applications involve more sophisticated processes, this simplification serves our pedagogical purpose of illustrating the fundamental properties of Fourier basis functions.

For each scenario, we generate T = 1000 time periods with N = 500 cross-sectional observations per period. We approximate the log-density using a Fourier series expansion with one sine and one cosine term:

$$\log \hat{f}_t(r) = z_{1,t} \sin(\kappa r) + z_{2,t} \cos(\kappa r) - \log C(\mathbf{z}_t),$$

where  $\kappa$  is the frequency parameter and  $C(\mathbf{z}_t)$  is the normalizing constant. The coefficients  $z_{1,t}$  (sine) and  $z_{2,t}$  (cosine) are estimated via maximum likelihood for each cross-section.

Figure 2 presents the key results across three panels that systematically demonstrate the distinct roles of Fourier basis components.

Panel A: Symmetric DGP (Cosine Captures Volatility) shows the symmetric DGP case where only volatility varies over time. The cosine coefficient  $z_{2,t}$  (red line) closely tracks the time-varying volatility

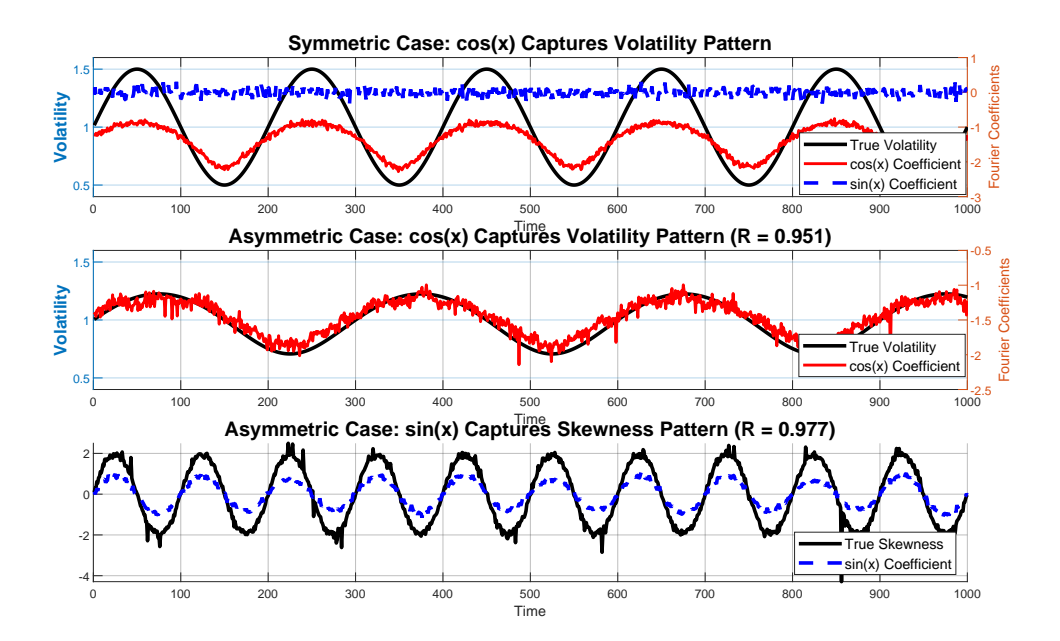


Figure 2: Simulation Study: Specialized Roles of Fourier Basis Functions. **Panel A:** In symmetric DGP (volatility-only), cosine coefficient tracks volatility while sine coefficient remains negligible. **Panel B:** In asymmetric DGP, cosine coefficient continues to capture volatility changes despite concurrent skewness variation. **Panel C:** In asymmetric DGP, sine coefficient specifically captures time-varying skewness pattern. Correlation coefficients (R) demonstrate strong relationships between basis coefficients and their respective distributional features.

pattern (black line), while the sine coefficient  $z_{1,t}$  (blue dashed line) remains negligible throughout.

Panel B: Asymmetric DGP (Cosine Captures Volatility) demonstrates that in the presence of both volatility and skewness variation, the cosine coefficient continues to faithfully capture volatility changes. Despite the introduction of time-varying skewness, the cosine component maintains its strong relationship with volatility (R > 0.95), showing that symmetric features are robustly encoded in cosine coefficients regardless of concurrent asymmetric dynamics.

Panel C: Asymmetric DGP (Sine Captures Skewness) reveals the specialized role of sine components in capturing distributional asymmetry. The sine coefficient  $z_{1,t}$  (blue dashed line) exhibits strong comovement with the time-varying skewness (black line), with positive sine coefficients corresponding to positive skewness and negative coefficients to negative skewness. The high correlation (R > 0.97) demonstrates that asymmetric distributional features are naturally and precisely encoded in the sine components.

This three-panel demonstration provides compelling visual evidence for the specialized roles of Fourier basis functions. The mathematical properties of these functions-cosine being even  $(\cos(-x) = \cos(x))$  and sine being odd  $(\sin(-x) = -\sin(x))$ -align perfectly with the symmetric and asymmetric characteristics of return distributions. This alignment provides an interpretable decomposition where:

- Cosine coefficients exclusively capture symmetric changes (volatility, dispersion)
- Sine coefficients specifically capture asymmetric changes (skewness, distributional shape)

The clean separation of effects across DGPs validates that our functional approach can separately identify these distinct aspects of distributional dynamics, which is crucial for understanding how different types of economic shocks affect financial markets.

Bjørnland et al. (2023) use functional PCA to span the return distribution in a Hilbert space and interpret the leading components as stability, tail-risk, and asymmetry factors. These interpretations are intuitive and supported by plots of the associated density shifts. However, because functional principal components are data-driven objects chosen solely to maximise explained variance, their shapes and consequently their economic meaning, are inherently sample-dependent and identified only up to sign (and, when eigenvalues are close, up to rotations). As a result, features such as skewness or tail behaviour may load across several components, making the interpretation of any single factor somewhat fragile. Our Fourier representation likewise spans the same Hilbert space, but does so using pre-specified cosine and sine functions. This provides a decomposition directly aligned with symmetric and asymmetric components of the distribution, yielding factors whose interpretation is stable across markets and over time, rather than relying on ex-post inspection of sample-specific eigenfunctions.

Building on the insights from the simulation study, we apply the Fourier basis to real-world financial returns. Consistent with the theoretical interpretation and controlled experiments, the cosine coefficient captures symmetric features of returns, co-moving with market volatility and acting as an endogenous volatility factor. The sine coefficient, by contrast, captures distributional asymmetry, with average values ordered United States > Euro area > Asia, reflecting well-documented regional differences in return skewness. Together, these factors provide a robust and economically meaningful separation of symmetric and asymmetric components, demonstrating that the interpretable decomposition observed in simulations carries over to actual market data. Details are in Appendix C.2.

#### 2.3.3 Practical Considerations

The idea that variations across stock markets can be effectively modeled using a small number of factors is both intuitive and practical, as it simplifies the complex dynamics of financial systems while retaining their key features. However, determining the optimal number of factors is crucial to accurately capturing the evolving return distributions across markets and over time. In the case of the skew-t distribution, which relies on a parametric assumption about the underlying distribution, the factors are naturally interpreted as the time-varying parameters, offering a straightforward approach to dynamic modeling. On the other hand, mvfVAR provides a more flexible framework where the model itself does not prescribe the number of factors but allows the data to inform this critical choice. This data-driven selection is achieved through cross-validation, which evaluates model performance to guide the choice of factor dimensionality.

Under the i.i.d. assumption, the dataset is partitioned into estimation and validation subsets. For model estimation, a randomly selected 75% of constituents per index is used to estimate the time-varying factors and constant factor loadings. The remaining 25% of constituents per index serves as the validation set, with performance measured by the sum of log-likelihoods across indices and over time. As shown in Table 1 shows that the model with  $r_1 = 6$ , the number of basis functions, achieves a higher log likelihood compared to specifications with  $r_1 = 2$  or  $r_1 = 4$ . For  $r_2$ , the log-likelihood values for one and two are quite similar, with the former offering a more parsimonious dimensionality. Given this marginal difference, we adopt  $r_1 = 6$ ,  $r_2 = 2$  in the main analysis to accommodate potential nonlinearities.

Table 1: Log likelihood for cross-validation ( $\times 10^6$ ).

			$r_2$	
		1	2	3
	2	-3.238	-	-
$r_1$	4	-2.960	-3.062	-3.082
	6	-2.730	-2.776	-2.874

#### 2.4 Summary of Out-of-Sample Performance

To explore potential advantages of distributional features from global stock markets in enhancing the forecast accuracy of the U.S. macroeconomy, and to assess whether our proposed model captures key characteristics of return distributions, we conduct a forecasting exercise using the monthly data presented in the Appendix B. The forecast performance of models is evaluated from Jan 2003 till the April 2025. Root mean squared forecast errors (RMSFEs) are used to evaluate the quality of point forecasts and averages of log predictive likelihoods (ALPLs) are used to evaluate the quality of density forecasts. Four models are considered: the first model is a VAR, served as the benchmark, stacking 15 overall indices and the U.S. macro. The second model is the proposed sktVAR model stacking skew t parameters (60 factors) and the macro. The third model is our proposed mvfVAR model where factors are produced from 15 stock market return distributions. The fourth model is a variant of mvfVAR, but based solely on the S&P 500 index.

Appendix D reports our forecasting results. When predicting macroeconomic aggregates, both mvf-VAR and sktVAR consistently outperform VAR in terms of data fit. This demonstrates that incorporating distributional features, rather than relying solely on aggregate indices, provides significant advantages in forecasting the macroeconomy. Additionally, mvfVAR, which accounts for the entire distribution of the data, surpasses the performance of models that include sktVAR, highlighting the value of a more comprehensive approach to distributional modeling. To assess the predictive accuracy of stock return distributions,

we compare the quantile scores generated by sktVAR and mvfVAR. While the two approaches show minimal differences when forecasting middle quantile scores, the divergence becomes more pronounced at the extremes. Specifically, mvfVAR consistently outperforms sktVAR in forecasting both upper and lower quantile scores, with its advantage being particularly notable in the lower quantiles. Although the skew-t distribution is sufficiently flexible to capture unimodal distributions and asymmetric features, it falls short in addressing more complex behaviours, such as bimodality. In contrast, mvfVAR excels in such scenarios, effectively capturing bimodal patterns that emerge during periods of heightened market divergence and uncertainty(Han, 2022). These bimodal behaviours often reflect shifts in market sentiment, driven by the diverse sectoral representation of larger stock markets. This ability to model the nuances of extreme market conditions further underscores mvfVAR's superiority in capturing the full distributional dynamics of stock returns. Finally, considering global indices is helpful to improve the forecasting performance compared to focusing solely on the US.

While we have explored two formulations, the out-of-sample performance strongly favours the mvfVAR model, indicating its superior predictive power. As a result, we base our subsequent structural analysis in Section 3 and 4 on this model.

# 3 US Monetary Policy Shock—Global market response

The neutrality of monetary policy has been a longstanding debate among financial economists (Thorbecke, 1997). According to pricing theory, stock prices reflect the expected present value of future net cash flows. Therefore, if contractionary monetary shocks lead to lower stock returns, it suggests that tighter monetary policy has real effects, either by reducing future cash flows or by increasing the discount rates used to value them. This section contributes to the discussion by analyzing how stock returns react to monetary policy shocks, providing empirical insights into their market impact. Instead of relying on a traditional single index (Bjørnland and Leitemo, 2009) or a portfolio of asset returns (Thorbecke, 1997), our model captures the full cross-sectional distribution, allowing for a more comprehensive assessment of how monetary policy influences the entire spectrum of market behaviour.

To identify the shock, we follow the approach of Bjørnland and Leitemo (2009), assuming that monetary policy has no long-run effect on real stock prices—a common long-run neutrality assumption. The key difference in our analysis is the inclusion of a vector of stock market factors, as opposed to a single factor in their framework. To address this, we impose further restrictions among the stock market factors by adopting a simple Cholesky decomposition and enforcing a long-run zero restriction on the responses of these factors to the monetary policy shock. Impulse response functions (IRFs) are from our proposed mvfVAR model with one lag in the VAR. Firstly, we find the responses of the macro variables (reported in Appendix E) to a monetary policy shock are consistent with standard macroeconomic theory: a contractionary monetary policy shock induces a contraction in output, and a reduction in prices. These findings are consistent with theoretical expectations and help validate the robustness and accuracy of our model. Interestingly, we do not find a J-curve for trade balance.<sup>3</sup> Our finding reveals a strong fast effect, followed by a gradual long-term normalization. This aligns with modern financial market dynamics, wherein short-term capital flows exert a dominant influence on immediate external balance responses, while longer-run adjustments

<sup>&</sup>lt;sup>3</sup>For example, Kim (2001) finds that following an expansionary monetary policy shock, the trade balance would first worsen for about one year, then improve. Given the symmetry inherent in standard VAR models, a similar but reversed pattern would be expected for a contractionary monetary shock.

unfold through real-sector channels. The absence of a J-curve suggests that financial globalization has fundamentally altered the transmission mechanism of monetary policy to trade flows.

Our focus here is on the functional impulse response functions (FIRFs). In a linear VAR framework that incorporates only the stock index, contractionary and expansionary monetary policy shocks will exhibit symmetric effects, merely shifting the index in opposite directions. Our framework enables us to uncover asymmetric effects of contractionary and expansionary monetary policy shocks, even at the cross-sectional mean of returns as it is no longer a linear mapping of the structural shocks. Unlike a standard linear VAR that assumes symmetric responses, our approach captures differences in magnitude, persistence, and market segmentation between the two directional shocks, revealing that contractionary policy tends to have a stronger and more immediate impact on stock returns, while expansionary policy generates a more gradual and muted effect. The FIRFs for log density can be obtained directly from the model (see Equation 2). Table 2 reports the changes for the first four moments of the distributions: mean, variance, skewness, and kurtosis.

- Contractionary U.S. monetary policy reduces stock market indices by raising interest rates, increasing borrowing costs, and lowering corporate profits. Higher yields make equities less attractive, prompting a market shift consistent with Bjørnland and Leitemo (2009); Thorbecke (1997). Tighter liquidity dampens sentiment, slowing economic activity. Crucially, these effects are heterogeneous across equity classes: growth-oriented stocks (e.g., NASDAQ constituents) exhibit asymmetric sensitivity, declining less during monetary tightening but rallying more aggressively during easing cycles—a pattern attributable to their longer-duration cash flows and higher elasticity to discount rate changes.
- These domestic equity market dynamics propagate globally through integrated financial markets. Higher U.S. yields trigger capital repatriation from foreign markets (Rey, 2015), further amplified by that international investors recalibrate growth forecasts based on U.S. monetary policy signals (Miranda-Agrippino and Rey, 2020).
- The positive values from 'Variance' column indicate that a positive monetary policy shock boost the stock market volatility as found in Bomfim (2003). We are finding that contractionary shocks elevate the variance more than expansionary shocks reduce it. This asymmetry aligns with the Federal Reserve's tendency to cushion market downturns while allowing rallies to persist, as documented by Rigobon and Sack (2003). The heightened volatility response to tightening shocks suggests that investors perceive monetary contractions as more disruptive to market stability than expansions are beneficial, reflecting an asymmetric risk perception in financial markets. While broadly consistent with this pattern, the Shanghai Stock Exchange exhibits slightly lower volatility responses compared to other major markets. This modest difference likely reflects China's use of countercyclical policies aimed at stabilizing domestic growth. The relative resilience of Chinese equities suggests that they may offer a limited hedge against volatility arising from U.S. monetary tightening, providing investors with a potential, though partial, risk diversification channel.
- There is little academic research on how monetary policy affects the higher moments of return distributions, but our finding suggest that Asian equity markets are more vulnerable compared to their European counterparts. This likely reflects differences in sectoral composition. Relative to Europe, indices in Japan, Korea, and China are more heavily concentrated in cyclical and export-oriented sectors—such as technology, manufacturing, and consumer electronics—which are more vulnerable to

- U.S. monetary tightening. This structural exposure amplifies downside risk and contributes to the observed asymmetry in return distributions.
- The Oslo Stock Exchange responded sharply to U.S. monetary policy, reflecting its sensitivity to global financial conditions and commodity markets. Norway's economy, heavily reliant on oil exports, faced further volatility as higher U.S. rates often dampen global demand expectations, leading to declining oil prices.

Table 2: Changes in the four moments of return distributions at horizon h = 0.

	Mean		Volatility		Skewness		Kurtosis	
	Expansionary	Contractionary	Expansionary	Contractionary	Expansionary	Contractionary	Expansionary	Contractionary
S&P 500	0.26	-0.18	-0.01	0.33	-0.57	-0.01	-3.34	-3.4
	(0.01, 0.47)	(-0.42, -0.05)	(-0.01, -0.01)	(0.27, 0.36)	(-1.58, 0.25)	(-0.07, 0.12)	(-3.42, -3.06)	(-3.41, -3.36)
NASDAQ	0.32	-0.17	-0.14	0.15	-0.8	0.13	2.93	-0.19
	(0.12, 0.46)	(-0.27, -0.07)	(-0.15, -0.12)	(0.11, 0.18)	(-2.20, -0.27)	(0.07, 0.18)	(1.07, 9.49)	(-0.21, -0.16)
FT All Share	0.1	-0.12	-0.07	0.29	0.09	0.02	0.21	-0.62
	(-0.08, 0.29)	(-0.23, -0.04)	(-0.07, -0.07)	(0.25, 0.30)	(-0.53, 0.74)	(-0.03, 0.07)	(-0.56, 2.90)	(-0.63, -0.61)
Europe 600	0.14	-0.11	-0.1	0.25	-0.01	0.01	2.57	-0.4
•	(0.01, 0.29)	(-0.19, -0.02)	(-0.10, -0.10)	(0.22, 0.27)	(-0.54, 0.39)	(-0.03, 0.06)	(-0.07, 6.18)	(-0.41, -0.38)
EURO STOXX	0.14	-0.11	-0.1	0.25	Ò	0.01	2.64	-0.39
	(0.01, 0.28)	(-0.19, -0.02)	(-0.10, -0.10)	(0.22, 0.27)	(-0.53, 0.41)	(-0.03, 0.06)	(-0.06, 6.22)	(-0.40, -0.38)
German	0.14	-0.1	-0.13	0.23	-0.1	0.02	4.89	-0.29
	(0.02, 0.28)	(-0.18, -0.03)	(-0.13, -0.12)	(0.20, 0.24)	(-0.57, 0.23)	(-0.01, 0.06)	(0.87, 6.39)	(-0.29, -0.27)
AEX All Share	0.14	-0.11	-0.12	0.24	-0.06	0.02	4.33	-0.32
	(0.02, 0.28)	(-0.18, -0.02)	(-0.12, -0.12)	(0.20, 0.25)	(-0.56, 0.29)	(-0.02, 0.06)	(0.44, 6.36)	(-0.33, -0.30)
Oslo	0.19	-0.11	-0.14	0.21	-0.47	0.05	5.04	-0.24
	(0.06, 0.34)	(-0.20, -0.05)	(-0.15, -0.14)	(0.19, 0.23)	(-1.03, -0.12)	(0.02, 0.10)	(2.77, 6.43)	(-0.24, -0.22)
SBF 120	0.14	-0.11	-0.11	0.24	-0.05	0.02	3.75	-0.35
	(0.01, 0.28)	(-0.19, -0.02)	(-0.11, -0.11)	(0.21, 0.26)	(-0.56, 0.31)	(-0.02, 0.06)	(0.22, 6.33)	(-0.35, -0.33)
DS Australia	0.13	-0.1	-0.12	0.23	-0.05	0.02	4.55	-0.31
	(0.01, 0.27)	(-0.18, -0.02)	(-0.12, -0.12)	(0.20, 0.25)	(-0.54, 0.31)	(-0.02, 0.06)	(0.59, 6.34)	(-0.31, -0.29)
Australia	0.18	-0.1	-0.14	0.21	-0.41	0.04	4.98	-0.23
	(0.06, 0.33)	(-0.19, -0.04)	(-0.15, -0.14)	(0.19, 0.22)	(-0.91, -0.08)	(0.01, 0.09)	(2.87, 6.27)	(-0.24, -0.22)
Nikkei	0.13	-0.1	-0.13	0.23	-0.06	0.02	4.92	-0.28
	(0.02, 0.27)	(-0.17, -0.02)	(-0.13, -0.13)	(0.19, 0.24)	(-0.53, 0.27)	(-0.02, 0.06)	(0.92, 6.52)	(-0.29, -0.27)
Горіх	0.17	-0.1	-0.14	0.22	-0.26	0.03	5.07	-0.26
•	(0.03, 0.28)	(-0.19, -0.03)	(-0.14, -0.13)	(0.19, 0.23)	(-0.62, 0.09)	(-0.00, 0.07)	(1.63, 6.35)	(-0.26, -0.24)
Korea	0.16	-0.1	-0.14	0.21	-0.22	0.03	5	-0.23
	(0.03, 0.27)	(-0.18, -0.03)	(-0.15, -0.14)	(0.18, 0.22)	(-0.59, 0.10)	(-0.00, 0.07)	(2.23, 6.28)	(-0.24, -0.22)
SHANGHAI SE	0.17	-0.1	-0.16	0.19	-0.29	0.04	4.7	-0.19
	(0.04, 0.28)	(-0.17, -0.03)	(-0.17, -0.15)	(0.17, 0.20)	(-0.65, 0.01)	(0.01, 0.07)	(2.73, 6.43)	(-0.19, -0.17)

Values in the brackeet are the 16% and 84% confidence intervals. In order to optimize space utilization, a series of abbreviations were employed, each representing: Europe 600 for STOXX Europe 600, German for German total market, Oslo for Oslo Exchange All Share, DS Australia for DS total market Australia, Australia for Australia All ordinaries, Nikkei for Nikkei 225 Stock, Korea for Korea Stock Exchange.

While we impose long-term zero restrictions on the effect of monetary policy shocks, ensuring that their influence is constrained over an extended horizon, our analysis reveals that the impact of these shocks on global stock markets dissipates within a relatively short timeframe, see Table 8and 9 in Appendix. Specifically, the effect on mean calms down quickly (after 1 month), suggesting that the transmission of monetary policy shocks to equity markets operates primarily over a shorter-term horizon. Higher moments need a little more time and the effect becomes negligible after nine months. This finding underscores the transient nature of monetary policy's influence on global stock market dynamics.

Complementing the Fourier basis results, our skew-t distribution analysis yields consistent patterns: expansionary shocks increase output, inflation, trade balances, and equity prices. Notably, the VAR model reveals symmetric responses for mean and skewness changes - contractionary shocks reduce these variables with magnitudes mirroring expansionary effects. For volatility and kurtosis, logarithmic transformations in the VAR specification produce asymmetric responses to large shocks in initial periods, while maintaining symmetry in their underlying positive domains.<sup>4</sup>

<sup>&</sup>lt;sup>4</sup>We compute the IRFs of volatility and kurtosis by: suppose  $z_t$  denotes volatility/kurtosis, let  $y_t = \log(z_t)$ , that is  $z_t = e^{y_t}$ . Then the IRF for  $z_t$  is  $\mathbb{E}\left[z_t|\operatorname{shock}\right] - \mathbb{E}\left[z_t|\operatorname{no shock}\right] = \exp\left(\mathbb{E}\left[y_t|\operatorname{shock}\right]\right) - \exp\left(\mathbb{E}\left[y_t|\operatorname{no shock}\right]\right) = \exp\left(\operatorname{IR}F_{yt} + \log z_0\right) - \exp\left(\log z_0\right) = z_0\left(e^{\operatorname{IR}F_y} - 1\right)$ .  $z_0$  is the pre-shock level of z.

# 4 From Deficits to Dispersion: The Sectoral and Policy Implications of U.S. Trade Balance

As the U.S. enters 2025 with a projected trade deficit of 3.2% of GDP (Congressional Budget Office, 2024), fundamental changes in global trade patterns are reshaping how external imbalances transmit to financial markets and monetary policy. Three structural shifts—shortening global technology supply chains, reconfiguration of energy trade flows, and productivity ambiguities from nearshoring (Freund et al., 2024)—have altered traditional transmission mechanisms and sectoral sensitivities to trade shocks. Early 2025 market data confirm this realignment: technology equities have underperformed historical norms, while energy and financial stocks have outperformed during periods of widening trade deficits.

These developments underscore the limitations of analyzing trade through net balances alone. The same trade deficit can mask fundamentally different underlying economic conditions—whether driven by weak external demand or strong domestic absorption—with distinct implications for inflation, output, and financial stability. We therefore analyze these dynamics through a conditional forecasting framework that separately identifies the effects of export and import shocks within a unified VAR model, providing a more nuanced understanding of how trade composition, rather than just net balances, affects the macroeconomy.

We estimate a Bayesian VAR containing five key U.S. variables: industrial production (IP), CPI inflation, exports, imports, and the federal funds rate. Using the conditional forecasting approach of (Chan et al., 2024), we conduct two distinct forecasting exercises that leverage Congressional Budget Office projections for 2025 (from May to October 2025).<sup>5</sup> The first exercise imposes the CBO's export path, fixing the import at the current value while allowing other variables to respond endogenously, cleanly identifying external demand shocks. The second imposes the CBO's import path and fixing export at the current value, capturing domestic absorption shocks. This unified framework ensures consistent parameter estimates and error structure across both exercises, providing a robust basis for comparing how different trade components transmit through the economy.

## 4.1 The Macroeconomic Propagation of a Negative Export Shock

Figure 3 left panel examines how a negative export shock propagates through the economy, illustrating a transmission mechanism that accords with standard open-economy theory. The immediate effect is a contraction in industrial production (INDPRO, top panel), as reduced external demand lowers the level of domestic output. This decline opens a negative output gap, which in turn generates a clear but moderate disinflationary impulse. The conditional path for CPI inflation lies up to 0.8 percentage points below its unconditional projection, suggesting a meaningful although not destabilizing reduction in inflationary pressures.

The response of monetary policy provides an informative perspective on the magnitude of the shock. The conditional forecast for the federal funds rate (FFR, bottom panel) falls below the baseline but only modestly so, indicating a more accommodative stance that remains well within the bounds of policy gradualism. This muted adjustment is consistent with a Taylor-type policy rule (Clarida et al., 2000): a pure demand shock that depresses both output and inflation warrants a reduction in the policy rate, but the extent of easing is proportional to the size of these deviations. Given the limited scale of the disinflation, a forceful easing cycle is neither required nor optimal. This behavior aligns with a monetary authority intent on maintaining

 $<sup>^5</sup>$ The porjection is available here https://www.cbo.gov/publication/61236. The project is quarterly and we convert to a monthly frequency using linear interpolation.

well-anchored inflation expectations and avoiding excessive responses to transitory disturbances (Bernanke, 2007).

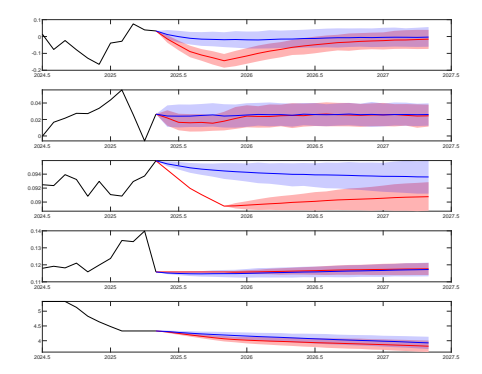
## 4.2 The Domestic Adjustment to a Negative Import Shock

We now contrast the previous analysis by considering a shock to domestic demand, imposed by conditioning the model on a path of declining import growth while holding exports fixed at their current level. This arrangement isolates a contraction in domestic absorption from movements in external demand. The resulting dynamics, shown in right panel, reveal a more intricate adjustment process than in the export shock scenario.

The conditional forecast (red lines) for industrial production displays a notably different profile: output initially rises above the unconditional path (blue) for roughly ten periods before converging. This early expansion is consistent with short-run import substitution and inventory adjustment, whereby domestic producers temporarily replace goods that would otherwise have been imported. As this substitution effect fades and weaker domestic demand takes hold, output gradually slips slightly below the unconditional projection. The overall pattern underscores the presence of offsetting short-run and medium-run forces absent in the export shock case.

Inflation dynamics similarly exhibit a two-stage adjustment. CPI inflation rises briefly above the baseline, reflecting transient cost-push pressures stemming from reduced import availability. This effect is short-lived and is quickly overtaken by the disinflationary consequences of a negative output gap. The conditional inflation path therefore falls below the unconditional forecast for most of the horizon, mirroring but not matching the magnitude of the response under the export shock.

The monetary policy response is strikingly modest. The conditional federal funds rate path is virtually identical to the unconditional one, indicating that the central bank perceives little need for meaningful adjustment. The opposing elements of the shock—temporary inflationary pressures combined with only mild and partially offsetting output effects—leave the optimal policy rate largely unchanged. As before, this outcome reflects a reaction function that emphasizes policy smoothing and the preservation of well-anchored expectations.



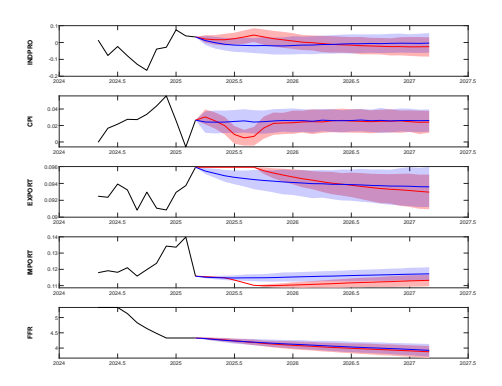


Figure 3: Left panel: Macroeconomic Effects of Export Conditioning. Conditional forecasts (red) imposing CBO export projections versus unconditional forecasts (blue). Right panel: Macroeconomic Effects of Import Conditioning. Conditional forecasts (red) imposing CBO import projections versus unconditional forecasts (blue).

#### 4.3 Financial market implications

Table 3 reveals striking heterogeneity in how global equity markets price tail risks from U.S. trade shocks, with clear patterns driven by sectoral composition and economic structure.

Technology Concentration Drives Extreme Vulnerability: The NASDAQ exhibits by far the largest Expected Shortfall estimates (conditional ES: -4.94% to -5.96%), reflecting technology stocks' unique sensitivity to demand shocks. This magnitude—approximately 15-20 times larger than the S&P 500's—stems from several factors: high operating leverage amplifies earnings sensitivity to revenue fluctuations, elevated valuation multiples compound price impacts, and global supply chain dependencies create complex transmission channels. South Korean equities, similarly concentrated in semiconductors and technology exports, show comparable vulnerability (-4.27% to -4.44% ES), confirming this as a sectoral rather than geographic phenomenon.

Commodity Exporters Face Significant Exposure: Oslo (-2.65% to -2.75% ES) and Australian markets (-3.34% to -3.55% ES) display substantial tail risk, consistent with commodity exporters' sensitivity to global demand fluctuations. The divergence between these two resource-heavy markets likely reflects composition differences: Australia's broader mining sector versus Norway's energy concentration. Both, however, significantly outperform the technology-heavy indices, suggesting different transmission mechanisms for commodity versus tech trade shocks.

European Markets Show Moderate, Homogeneous Risk: Major European indices cluster in a narrow band (-0.94% to -1.53% ES), with remarkable consistency across regional (Europe 600, EURO STOXX) and national (German, French, Dutch) benchmarks. This homogeneity suggests deeply integrated capital markets and similar sectoral exposures across European economies. Germany's slightly elevated risk (-1.39% to -1.45% ES) may reflect its greater export orientation within the European bloc.

U.S. Diversification Provides Exceptional Resilience: The S&P 500's remarkably low ES estimates (-0.24% to -0.32% ES)—an order of magnitude smaller than the NASDAQ's—highlights the powerful diversification benefits of broad market exposure. While specific sectors face substantial trade vulnerability, the aggregate U.S. market appears well-insulated, likely due to its domestic demand orientation and sectoral balance.

China's Moderate Risk Challenges Conventional Narratives: The Shanghai Composite's midrange vulnerability (-2.11% to -2.26% ES) contradicts crisis narratives about Chinese financial fragility. Several factors may explain this resilience: capital controls insulate domestic markets from sudden outflows, policy buffers allow rapid response to external shocks, and the market's retail investor base may be less sensitive to trade fundamentals than institutional investors in developed markets.

The clear sectoral patterns—technology extreme risk, commodities significant risk, diversified moderate risk—suggest that trade shock transmission operates primarily through industrial channels rather than broad financial contagion. This has important implications for portfolio construction and risk management, particularly the value of cross-sectoral diversification in mitigating trade-related tail risks.

# 5 Conclusion

This paper proposes incorporating distributional features of global financial markets into a macroeconomic model. The analyses explore and provide insights into the complex dependence between global stock markets and U.S. economic conditions. We find two-way spillovers. One is the significant functional impulse

Table 3: Expected Shortfall at h = 0.

	Positive de	emand shock	Negative d	emand shock
	Conditional	Unconditional	Conditional	Unconditional
S\&P 500	-0.32	-0.29	-0.29	-0.24
NASDAQ	-4.94	-4.81	-5.96	-5.61
FT All Share	-1.17	-1.12	-1.06	-0.96
Europe 600	-1.11	-1.05	-0.99	-0.94
EURO STOXX	-1.12	-1.06	-0.99	-0.94
German	-1.45	-1.39	-1.33	-1.28
AEX All Share	-1.60	-1.53	-1.46	-1.40
Oslo	-2.75	-2.65	-2.72	-2.61
SBF 120	-0.98	-0.94	-0.80	-0.75
DS Australia	-1.23	-1.18	-1.11	-1.06
Australia	-3.55	-3.42	-3.47	-3.34
Nikkei	-1.85	-1.77	-1.69	-1.63
Topix	-1.92	-1.84	-1.80	-1.74
Korea	-4.44	-4.27	-4.18	-4.04
SHANGHAI SE	-2.26	-2.18	-2.16	-2.11

response functions to a U.S. monetary policy shock, particularly a reduction in mean returns and a slight increase in volatility, with the Shanghai Stock Exchange as the exception, exhibiting a contrasting upward trend. These findings highlight the varying sensitivities of global markets to U.S. policy shifts, driven by differences in market structures, capital controls, and economic linkages. Additionally, our conditional forecasts based on CBO projections reveal differentiated effects of demand shocks. Export-driven external shocks trigger conventional contractions and disinflation, while import-driven domestic shocks produce nuanced adjustments—including short-term import substitution, transient cost-push pressures, and mild disinflation—accompanied by modest monetary responses. Mapping these shocks to expected equity short-falls shows pronounced heterogeneity: technology-heavy indices are highly vulnerable, commodity exporters face distinct exposure, diversified benchmarks like the S&P 500 are resilient, and China occupies an intermediate position.

These findings demonstrate that trade-shock transmission operates through sharply sector-specific channels, underscoring the importance of integrating macroeconomic dynamics with financial tail risks. Recognizing these interdependencies is crucial for policymakers to anticipate the macroeconomic consequences of market fluctuations and design effective responses to global financial shocks, offering a more nuanced perspective on financial stability and policy formulation.

# References

Azzalini, A. and Capitanio, A. (2003). Distributions generated by perturbation of symmetry with emphasis on a multivariate skew t-distribution. *Journal of the Royal Statistical Society Series B: Statistical Methodology*, 65(2):367–389.

Bai, J. and Wang, P. (2015). Identification and bayesian estimation of dynamic factor models. *Journal of Business & Economic Statistics*, 33(2):221–240.

Bernanke, B. (2007). Inflation expectations and inflation forecasting. Technical report, Board of Governors of the Federal Reserve System (US).

- Bjørnland, H. C., Chang, Y., and Cross, J. (2023). Oil and the stock market revisited: A mixed functional var approach. *Manuscript, BI Norwegian Business School and Indiana University*.
- Bjørnland, H. C. and Leitemo, K. (2009). Identifying the interdependence between us monetary policy and the stock market. *Journal of Monetary Economics*, 56(2):275–282.
- Bomfim, A. N. (2003). Pre-announcement effects, news effects, and volatility: Monetary policy and the stock market. *Journal of Banking & Finance*, 27(1):133–151.
- Boyd, S. P. and Vandenberghe, L. (2004). Convex optimization. Cambridge university press.
- Brunnermeier, M., Palia, D., Sastry, K. A., and Sims, C. A. (2021). Feedbacks: financial markets and economic activity. *American Economic Review*, 111(6):1845–1879.
- Chan, J. C. (2022). Asymmetric conjugate priors for large bayesian vars. *Quantitative Economics*, 13(3):1145–1169.
- Chan, J. C., Pettenuzzo, D., Poon, A., and Zhu, D. (2024). Conditional forecasts in large bayesian vars with multiple equality and inequality constraints. arXiv preprint arXiv:2407.02262.
- Chang, B. Y., Christoffersen, P., and Jacobs, K. (2013). Market skewness risk and the cross section of stock returns. *Journal of Financial Economics*, 107(1):46–68.
- Chang, M., Chen, X., and Schorfheide, F. (2024). Heterogeneity and aggregate fluctuations. Journal of Political Economy, 132(12):000–000.
- Clarida, R., Gali, J., and Gertler, M. (2000). Monetary policy rules and macroeconomic stability: evidence and some theory. *The Quarterly journal of economics*, 115(1):147–180.
- Congressional Budget Office (2024). The budget and economic outlook: 2025 to 2035. Report, Congressional Budget Office. Accessed July 2025.
- Crain, B. R. (1974). Estimation of distributions using orthogonal expansions. *The annals of statistics*, 2(3):454–463.
- Diebold, F. X. and Mariano, R. S. (2002). Comparing predictive accuracy. *Journal of Business & economic statistics*, 20(1):134–144.
- Diebold, F. X., Rudebusch, G. D., and Aruoba, S. B. (2006). The macroeconomy and the yield curve: a dynamic latent factor approach. *Journal of econometrics*, 131(1-2):309–338.
- Flannery, M. J. and Protopapadakis, A. A. (2002). Macroeconomic factors do influence aggregate stock returns. *The review of financial studies*, 15(3):751–782.
- Freund, C., Mattoo, A., Mulabdic, A., and Ruta, M. (2024). Is us trade policy reshaping global supply chains? *Journal of International Economics*, 152:104011.
- Geweke, J. (2001). Bayesian econometrics and forecasting. Journal of Econometrics, 100(1):11–15.
- Han, C. (2022). Bimodal characteristic returns and predictability enhancement via machine learning. Management Science, 68(10):7701–7741.

- Kelly, B. and Jiang, H. (2014). Tail risk and asset prices. The Review of Financial Studies, 27(10):2841–2871.
- Kim, S. (2001). International transmission of us monetary policy shocks: Evidence from var's. *Journal of monetary Economics*, 48(2):339–372.
- Menzly, L. and Ozbas, O. (2010). Market segmentation and cross-predictability of returns. *The Journal of Finance*, 65(4):1555–1580.
- Miranda-Agrippino, S. and Rey, H. (2020). Us monetary policy and the global financial cycle. *The Review of Economic Studies*, 87(6):2754–2776.
- Poon, S.-H., Rockinger, M., and Tawn, J. (2004). Extreme value dependence in financial markets: Diagnostics, models, and financial implications. *The Review of Financial Studies*, 17(2):581–610.
- Rey, H. (2015). Dilemma not trilemma: the global financial cycle and monetary policy independence. Technical report, National Bureau of Economic Research.
- Rigobon, R. and Sack, B. (2003). Measuring the reaction of monetary policy to the stock market. *The quarterly journal of Economics*, 118(2):639–669.
- Thorbecke, W. (1997). On stock market returns and monetary policy. *The Journal of Finance*, 52(2):635–654.
- Wang, D., Liu, X., and Chen, R. (2019). Factor models for matrix-valued high-dimensional time series. Journal of econometrics, 208(1):231–248.

# Appendices - for online publication only

# A Theoretical Results: Algorithm Convergence

The objective is non-convex in Z,  $\beta$  jointly due to their bilinear coupling, so alternating maximization could in principle stall, cycle, or converge to non-informative points without guarantees (Boyd and Vandenberghe, 2004). This section gives convergence result ensures monotone ascent and that any limit point is a stationary solution of the likelihood, which under our (standard) exponential-family assumptions further yields a linear rate—giving reliable stopping rules, runtime predictability, and reproducibility. It also clarifies which modeling choices (e.g., bounded bases like Fourier and compact parameter sets) are sufficient for these guarantees, guiding practical implementations.

**Assumption 1.**  $\{Z_t\}_{t=1}^T$  and  $\{\beta_m\}_{m=1}^M$  are restricted to a closed and convex set  $\mathcal{D}$  that is consistent with the identification restrictions.

**Assumption 2.** Let  $\Phi: \mathcal{X} \to \mathbb{R}^r$  be the basis vector. Assume all integrals are w.r.t. Lebesgue (or counting) measure and write

$$|S| := \int_{S} 1 \, dx > 0.$$

Suppose:

$$(A\Phi 1) \quad \|\Phi(x)\| \le B \quad \forall x,$$

$$(A\Phi 2) \quad \exists S \subseteq \mathcal{X} \text{ with } |S| > 0 \text{ such that} \quad \Sigma_S := \frac{1}{|S|} \int_S (\Phi(x) - \mu_S) (\Phi(x) - \mu_S)^\top dx \succeq \lambda_0 I,$$

$$\mu_S := \frac{1}{|S|} \int_S \Phi(x) dx, \qquad \lambda_0 > 0.$$

We first impose a uniform bound on the basis vector, keeping scores and Fisher information finite and yielding block-Lipschitz smoothness of the objective. Further, we require that on some subset S of positive measure the features are not collinear—i.e., their covariance is uniformly positive definite—so the Fisher information is bounded below.

These are **standard regularity conditions** for exponential families (bounded sufficient statistics and uniformly positive-definite information) used to ensure identifiability, well-posed MLEs, and the convergence guarantees of EM/coordinate-ascent and Newton-type methods. They are readily met by common bounded bases (Fourier, splines, orthogonal polynomials) on compact supports.

**Lemma 1.** For  $\theta \in \mathbb{R}^d$ , define

$$p_{\theta}(x) = \frac{\exp\{\Phi(x)^{\top}\theta\}}{\int \exp\{\Phi(u)^{\top}\theta\} du}, \qquad A(\theta) = \log\int \exp\{\Phi(u)^{\top}\theta\} du.$$

Then there exists  $\mu > 0$  such that, for all  $\theta \in \Theta$ ,

$$\nabla^2 A(\theta) \ = \ \mathrm{Var}_{p_\theta}[\Phi(X)] \ \succeq \ \mu I.$$

*Proof.* Let  $\Theta := \{Z_t \beta_m : (Z, \beta) \in \mathcal{D}, t, m\}$  and by Assumption 1  $\Theta$  is compact. Thus,

$$M:=\sup_{\theta\in\Theta}\|\theta\|<\infty.$$

Boundedness (A $\Phi$ 1) gives, for  $x \in S$ ,

$$e^{-BM} \le e^{\Phi(x)^{\top}\theta} \le e^{BM}.$$

Hence the probability of S under  $p_{\theta}$  is uniformly positive:

$$p_{\theta}(S) \geq \rho > 0, \quad \forall \theta \in \Theta.$$

Variance decomposition yields

$$\operatorname{Var}_{p_{\theta}}[\Phi] \succeq p_{\theta}(S) \operatorname{Var}_{p_{\theta}}[\Phi \mid X \in S].$$

Let r be the Lebesgue on S and  $q_{\theta} := p_{\theta}(\cdot \mid X \in S)$ , we have

$$e^{-2BM} \le \frac{dq_{\theta}}{dr} \le e^{2BM}$$

on S. By Assumption 2, it gives

$$\operatorname{Var}_{p_{\theta}}[\Phi \mid X \in S] = \operatorname{Var}_{q_{\theta}}[\Phi] \succeq e^{-2BM} \operatorname{Var}_{r}[\Phi] =: c(M, B) \operatorname{Var}[\Phi \mid X \in S].$$

Combining these bounds gives

$$\operatorname{Var}_{p_{\theta}}[\Phi] \succeq \underbrace{\rho c(M, B) \lambda_{0}}_{:=\mu} I, \quad \forall \theta \in \Theta.$$

The intuition of this result is that on some subset S of positive measure/mass, the components of the basis vector are **not collinear**—the covariance/Gram matrix is uniformly positive definite with minimal eigenvalue.

We now move on to identification, such that

$$\beta = \begin{bmatrix} I_{r_2} \\ \tilde{\beta} \end{bmatrix}.$$

Corollary 1. Under the identification scheme,

$$\mathcal{L}(Z,\beta) = \sum_{t=1}^{T} \sum_{m=1}^{M} \left[ \sum_{j=1}^{N_{m,t}} \Phi(y_{jmt})^{\top} Z_{t} \beta_{m} - N_{m,t} A(Z_{t} \beta_{m}) \right], \qquad A(\theta) = \log \int \exp\{\Phi(x)^{\top} \theta\} dx.$$

 $F := -\mathcal{L}$  is block-smooth and block-strongly convex, if there is no nonzero direction  $v \in \mathbb{R}^{r_1}$  such that for every t with  $N_{m,t} > 0$ ,

$$\log \frac{f_{i,t}(x)}{f_{i,t}(x)} = a_t + b_t v^{\top} \Phi(x) \quad \textit{for some } a_t, b_t \in \mathbb{R} \textit{ and all } x, i \neq j <= r_2.$$

*Proof.* Step 1 (The  $Z_t$ -block). Fix t. The negative Hessian with respect to  $Z_t$  is

$$-\nabla_{Z_t}^2 \ell_t = \sum_m N_{m,t} \left(\beta_m \otimes I\right) \nabla^2 A(Z_t \beta_m) \left(\beta_m^\top \otimes I\right).$$

By uniform convexity,

$$-\nabla_{Z_t}^2 \ell_t \succeq \mu \sum_m N_{m,t} \left(\beta_m \beta_m^\top \otimes I\right).$$

Since  $\{\beta_1,\ldots,\beta_{r_2}\}$  are the canonical basis vectors  $e_1,\ldots,e_{r_2}$  under the chosen identification, we obtain

$$\sum_{m=1}^{r_2} N_{m,t} \, \beta_m \beta_m^{\top} = \operatorname{diag}(N_{1,t}, \dots, N_{r_2,t}) \succeq N_{\min,t} \, I_{r_2},$$

where  $N_{\min,t} = \min_{1 \le m \le r_2} N_{m,t}$ . Thus

$$-\nabla_{Z_t}^2 \ell_t \succeq \mu N_{\min,t} \left( I_{r_2} \otimes I \right),$$

which shows that the  $Z_t$ -block is positive definite uniformly in t.

Step 2 (The  $\beta$ -block). The negative Hessian with respect to  $\beta_m$  is

$$-\nabla_{\beta}^2 \ell = \sum_t N_{m,t} Z_t^{\top} \nabla^2 A(Z_t \beta_m) Z_t \succeq \mu \sum_t N_{m,t} Z_t^{\top} Z_t.$$

Without the loss of generality, we shall examine  $r_2 = 2$  case such that

$$f_{1,t}(x) = \exp\left(\Phi(x)Z_{t,1} - A(Z_{t,1})\right) \quad f_{2,t}(x) = \exp\left(\Phi(x)Z_{t,2} - A(Z_{t,2})\right).$$

We have

$$\log\left(\frac{f_{1,t}(x)}{f_{2,t}(x)}\right) = \Phi(x)(Z_{t,1} - Z_{t,2}) - A(Z_{t,1}) + A(Z_{t,2}).$$

If there is collinearity in  $Z_t$ 's, we can write  $Z_{t,1} = cZ_{t,2}$ , the above expression becomes

$$\log\left(\frac{f_{1,t}(x)}{f_{2,t}(x)}\right) = (c-1)Z'_{t,2}\Phi(x) - A(cZ_{t,1}) + A(Z_{t,2})$$

which contracts the assumption. Consequently, the  $\beta$ -block is positive definite. Combining with Step 1,  $F = -\mathcal{L}$  is block-strongly convex. **Step 3** Note that the basis is uniformly bounded on the support:

$$\|\Phi(x)\|_2 \le B \quad \forall x \in \mathcal{X}.$$

For any  $\theta$  and any  $u \in \mathbb{R}^{r_1}$ ,

$$u^{\top} \nabla^2 A(\theta) u = \operatorname{Var}_{p_{\theta}}(u^{\top} \Phi(X)) \le \mathbb{E}_{p_{\theta}} [(u^{\top} \Phi(X))^2] \le ||u||_2^2 \, \mathbb{E}_{p_{\theta}} [||\Phi(X)||_2^2] \le ||u||_2^2 B^2.$$

Therefore  $\nabla^2 A(\theta) \leq B^2 I$  for all  $\theta$ . Consequently, the block Hessians satisfy

$$-\nabla_{Z_t}^2 \ell_t \preceq B^2 \sum_m N_{m,t} \left(\beta_m \beta_m^\top \otimes I\right), \qquad -\nabla_{\beta_m}^2 \ell \preceq B^2 \sum_t N_{m,t} Z_t^\top Z_t,$$

which provides uniform block-Lipschitz (block-smoothness) constants.

In our application, we rescale x to [0,1] and take  $\Phi(x) = (\cos 2\pi x, \sin 2\pi x, \dots, \cos 2\pi K x, \sin 2\pi K x)^{\top} \in \mathbb{R}^{2K}$ . First, each trigonometric component has magnitude  $\leq 1$ , so

$$\|\Phi(x)\|^2 = \sum_{k=1}^K \left(\cos^2(2\pi kx) + \sin^2(2\pi kx)\right) = 2K,$$

which yields a uniform bound  $B = \sqrt{2K}$ . This directly controls gradient/Hessian magnitudes and provides finite block Lipschitz constants for  $F = -\mathcal{L}$ . Secondly, on S = [0, 1] under the uniform measure,

$$Var[\Phi(X)] = \frac{1}{2}I_{2K},$$

so the Gram/covariance is strictly positive definite with  $\lambda_{\min} = \frac{1}{2}$ . This ensures directions in the span of  $\Phi$  are informative, preventing flat likelihood directions. With compact induced parameter set and  $\|\Phi(x)\| \leq B$ , we have a bounded exponential tilt on [0,1]. Standard comparison yields

$$\nabla^2 A(\theta) = \operatorname{Var}_{p_{\theta}}[\Phi(X)] \succeq \mu I \quad (\theta \in \Theta)$$

for some  $\mu > 0$ . Thus A is uniformly strongly convex over  $\Theta$ , giving block strong concavity of  $\mathcal{L}$  and enabling the linear convergence rate. The same boundedness implies

$$0 \ \le \ \nabla^2 A(\theta) \ \le \ B^2 I,$$

so block gradients of  $F = -\mathcal{L}$  are Lipschitz with finite constants  $(L_Z, L_\beta)$ , a standard requirement in rate analyses. In practice, choose a moderate K to keep the Gram well-conditioned; orthogonal trig functions already help. Ensure the data/quadrature grid covers [0,1] (or a nontrivial  $S \subset [0,1]$ ) so empirical covariances stay away from degeneracy.

**Assumption 3.** At each iteration, every block subproblem—optimizing over  $Z_t$  with  $\beta$  fixed or over  $\beta_m$  with Z fixed—is solved exactly, yielding the global maximizer within the feasible set.

**Proposition 1** (Convergence). Let  $\mathcal{L}(Z,\beta)$  be the objective and  $\{(Z^k,\beta^k)\}_{k\geq 0}$ , we have  $\mathcal{L}(Z^k,\beta^k)$  nondecreasing and bounded above, that implies  $\mathcal{L}(Z^k,\beta^k) \xrightarrow[k\to\infty]{} \mathcal{L}^{\star}$ .

Any cluster point  $(Z^*, \beta^*)$  satisfies block optimality:

$$Z_t^{\star} \in \arg\max_{Z_t \in \mathcal{D}} \mathcal{L}(Z, \beta^{\star}), \qquad \beta_m^{\star} \in \arg\max_{\beta_m \in \mathcal{D}} \mathcal{L}(Z^{\star}, \beta).$$

Equivalently, in variational/KKT form:

$$\langle \nabla_{Z_t} \mathcal{L}(Z^*, \beta^*), Z_t - Z_t^* \rangle \leq 0, \ \forall Z_t \in \mathcal{D}, \qquad \langle \nabla_{\beta_m} \mathcal{L}(Z^*, \beta^*), \beta_m - \beta_m^* \rangle \leq 0, \ \forall \beta_m \in \mathcal{D}.$$

If, moreover, Assumption 2 holds (uniform Fisher information  $\succeq \mu I$ ) and identification gives unique block maximizers, then

$$\nabla_{Z_t} \mathcal{L}(Z^\star, \beta^\star) = 0, \quad \nabla_{\beta_m} \mathcal{L}(Z^\star, \beta^\star) = 0 \quad \forall t, m,$$

so  $(Z^*, \beta^*)$  is stationary and the whole sequence converges to it.

*Proof.* First of all, the algorithm is by definition monotone descent

$$Z^{k+1} \in \arg\max_{Z} \mathcal{L}(Z, \beta^{k}) \implies \mathcal{L}(Z^{k+1}, \beta^{k}) \ge \mathcal{L}(Z^{k}, \beta^{k}),$$

$$\beta^{k+1} \in \arg\max_{\beta} \mathcal{L}(Z^{k+1}, \beta) \implies \mathcal{L}(Z^{k+1}, \beta^{k+1}) \ge \mathcal{L}(Z^{k+1}, \beta^{k}),$$

$$\implies \mathcal{L}(Z^{k+1}, \beta^{k+1}) \ge \mathcal{L}(Z^{k}, \beta^{k}) \quad \forall k \implies \{\mathcal{L}(Z^{k}, \beta^{k})\}_{k \ge 0} \nearrow.$$

$$(Z^{k}, \beta^{k}) \in \mathcal{D} \text{ (closed, bounded)}, \quad \Phi \text{ bounded} \implies \sup_{(Z, \beta) \in \mathcal{D}} \mathcal{L}(Z, \beta) < \infty.$$

$$\{\mathcal{L}(Z^k,\beta^k)\}_{k\geq 0} \nearrow, \sup_k \mathcal{L}(Z^k,\beta^k) \leq \sup_{(Z,\beta)\in\mathcal{D}} \mathcal{L}(Z,\beta) < \infty \Rightarrow \exists \mathcal{L}^* < \infty : \mathcal{L}(Z^k,\beta^k) \to \mathcal{L}^*.$$

Take a convergent subsequence:

$$(Z^{k_j}, \beta^{k_j}) \to (Z^{\star}, \beta^{\star}), \quad j \to \infty.$$

For the Z-update, each  $Z_t^{k_j+1}$  is the block maximizer:

$$Z_t^{k_j+1} \in \arg\max_{Z_t} \mathcal{L}(Z, \beta^{k_j}) \ \Rightarrow \ \mathcal{L}(Z^\star, \beta^{k_j}) \ \geq \ \mathcal{L}((Z_1^\star, \dots, \widetilde{Z}_t, \dots), \beta^{k_j}), \ \forall \widetilde{Z}_t.$$

For the  $\beta\text{--update,}$  each  $\beta_m^{k_j+1}$  is the block maximizer:

$$\beta_m^{k_j+1} \in \arg\max_{\beta_m} \mathcal{L}(Z^{k_j+1},\beta) \ \Rightarrow \ \mathcal{L}(Z^{k_j+1},\beta^*) \ \geq \ \mathcal{L}(Z^{k_j+1},(\beta_1^*,\ldots,\widetilde{\beta}_m,\ldots)), \ \forall \widetilde{\beta}_m.$$

Passing to the limit  $j \to \infty$  and using continuity of  $\mathcal{L}$  gives that no single-block change can improve the objective. We also have uniform strong convexity of the log-partition:

$$\nabla^2 A(\theta) \succeq \mu I$$
.

This implies strict concavity of  $\mathcal{L}$  in each block:

$$Z \mapsto \mathcal{L}(Z,\beta)$$
 strictly concave,  $\beta \mapsto \mathcal{L}(Z,\beta)$  strictly concave.

With the identification restrictions in place, each block maximizer is unique. Therefore, for any block-stationary point  $(Z^*, \beta^*)$ :

$$\nabla_Z \mathcal{L}(Z^*, \beta^*) = 0, \qquad \nabla_\beta \mathcal{L}(Z^*, \beta^*) = 0.$$

Hence  $(Z^*, \beta^*)$  is a stationary point. Uniqueness of block maximizers prevents cycling, so the entire sequence converges:

$$(Z^k, \beta^k) \rightarrow (Z^{\star}, \beta^{\star}).$$

**Theorem 1** (Convergence rate of alternating maximization). Let  $F := -\mathcal{L}$ . Suppose F is block-smooth

and block-strongly convex:

$$\|\nabla_Z F(Z,\beta) - \nabla_Z F(Z',\beta)\| \le L_Z \|Z - Z'\|, \qquad \|\nabla_\beta F(Z,\beta) - \nabla_\beta F(Z,\beta')\| \le L_\beta \|\beta - \beta'\|,$$

With  $\rho := (1 - \frac{\mu}{L_Z})(1 - \frac{\mu}{L_B}) \in (0, 1)$ 

$$\mathcal{L}^{\star} - \mathcal{L}(Z^k, \beta^k) \leq \rho^k \left[ \mathcal{L}^{\star} - \mathcal{L}(Z^0, \beta^0) \right].$$

*Proof.* Let  $F := -\mathcal{L}$ . For the Z—update at iteration k, fix  $\beta = \beta^k$  and set  $g_Z(Z) := F(Z, \beta^k)$ . By block  $L_Z$ —smoothness (descent lemma) and exact minimization,

$$g_Z(Z^{k+1}) \le g_Z(Z^k) - \frac{1}{2L_Z} \|\nabla_Z g_Z(Z^k)\|^2.$$

By  $\mu$ —strong convexity of  $g_Z$  and the Polyak–Łojasiewicz inequality,

$$\|\nabla_Z g_Z(Z^k)\|^2 \ge 2\mu [g_Z(Z^k) - \min_Z g_Z(Z)].$$

Combining,

$$g_Z(Z^{k+1}) - \min_Z g_Z \le \left(1 - \frac{\mu}{L_Z}\right) [g_Z(Z^k) - \min_Z g_Z].$$
 (Z)

For the  $\beta$ —update at the same iteration, fix  $Z = Z^{k+1}$  and set  $g_{\beta}(\beta) := F(Z^{k+1}, \beta)$ . By the same argument,

$$g_{\beta}(\beta^{k+1}) - \min_{\beta} g_{\beta} \leq \left(1 - \frac{\mu}{L_{\beta}}\right) \left[g_{\beta}(\beta^{k}) - \min_{\beta} g_{\beta}\right]. \tag{\beta}$$

Note  $\min_{Z} g_{Z} = \min_{Z} F(Z, \beta^{k}) \geq F^{*} := \min_{Z,\beta} F(Z, \beta)$  and  $\min_{\beta} g_{\beta} = \min_{\beta} F(Z^{k+1}, \beta) \geq F^{*}$ . Thus, from (Z),

$$F(Z^{k+1}, \beta^k) - F^* \le \left(1 - \frac{\mu}{L_Z}\right) [F(Z^k, \beta^k) - F^*],$$

and from  $(\beta)$ ,

$$F(Z^{k+1}, \beta^{k+1}) - F^{\star} \leq \left(1 - \frac{\mu}{L_{\beta}}\right) [F(Z^{k+1}, \beta^{k}) - F^{\star}].$$

Chaining the two displays gives the geometric decay in one full iteration:

$$F(Z^{k+1}, \beta^{k+1}) - F^{\star} \leq \underbrace{\left(1 - \frac{\mu}{L_Z}\right) \left(1 - \frac{\mu}{L_\beta}\right)}_{:= \rho < 1} \left[F(Z^k, \beta^k) - F^{\star}\right].$$

Equivalently for  $\mathcal{L} = -F$ ,

$$\mathcal{L}^{\star} - \mathcal{L}(Z^{k+1}, \beta^{k+1}) \leq \rho \left[ \mathcal{L}^{\star} - \mathcal{L}(Z^{k}, \beta^{k}) \right], \qquad \rho = (1 - \mu/L_{Z})(1 - \mu/L_{\beta}) \in (0, 1).$$

Iterating yields

$$\mathcal{L}^{\star} - \mathcal{L}(Z^k, \beta^k) \leq \rho^k \left[ \mathcal{L}^{\star} - \mathcal{L}(Z^0, \beta^0) \right].$$

# **B** Data Description

Table 4 provides details of the monthly dataset and transformations used in the empirical application.

Table 4: Monthly dataset of variables.

	Stock indices	
Market	Index	Transformation
U.S.	S&P 500	
U.S.	NASDAQ (Nasdaq Composite)	
UK	FT All Share (FTSE All Share)	
Europe	STOXX Europe 600	
Europe	EURO STOXX	
Germany	German total market	
Netherlands	AEX All Share	
Norway	Oslo Exchange All Share	$\triangle \log$
France	SBF 120	
Australia	DS total market Australia (Datastream)	
Australia	Australia All ordinaries	
Japan	Nikkei 225 Stock Average	
Japan	Topix	
South Korea	Korea Stock Exchange Composite	
China	SHANGHAI SE A SHARE	
	Macro variables	
	Variables (with FRED mnemonic)	Transformation
	Industrial Production Index (INDPRO)	$\triangle \log$
U.S.	Consumer Price Index (CPIAUCSL)	
	Trade Balance (BOPGSTB)	
	Federal Funds Rate	level

Note: For stock indices, we take the growth rate to neutralize influence of market capitalizations. And the growth is computed as annual growth  $12 * log(\frac{y_t}{y_{t-1}})$ . To make it consistent, the macro variables (except Federal Funds Rate) are transformed similarly.

# C Plots of extracted distributional features

## C.1 Scree plots of skew-t parameters

The 15 indices, with four parameters for each index, will lead to 60 parameters. To show those 60 parameters exhibit a low-dimensional representation, Figure 4 reports the scree plot for each parameter. The big gap or elbow is clearly seen in parameter scale and skewness.

# C.2 Extracted factors using the Fourier basis

This section complements the simulation study by examining the behavior of the Fourier-based factors in real data. Consistent with the theoretical arguments and controlled experiments presented above, we find that the estimated coefficients on the cosine and sine basis functions capture distinct features of financial returns, corresponding to volatility and asymmetry, respectively.

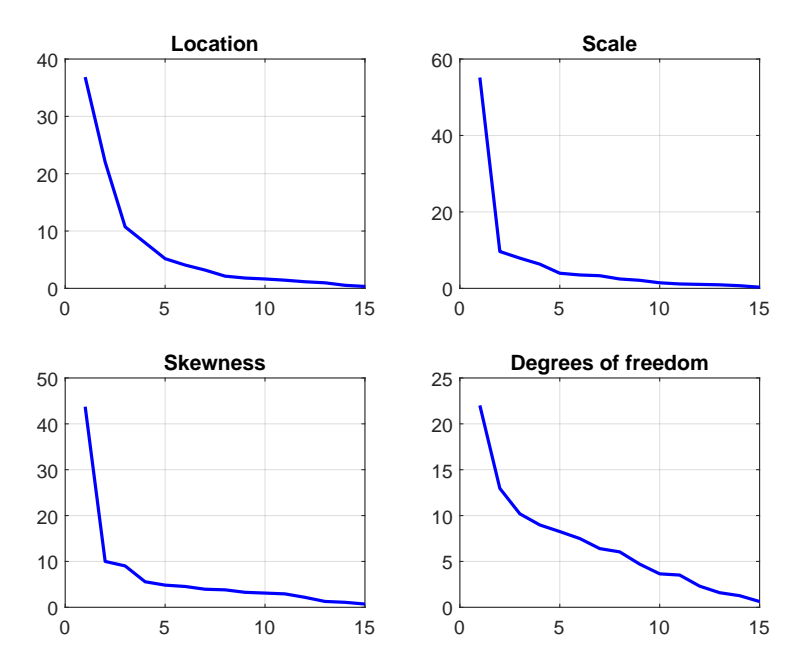


Figure 4: Scree plot of the four skew-t parameters. An elbow is shown in scale and skewness.

Figure 5 plots the time series of the cosine coefficient alongside the VIX index. The two series exhibit striking co-movement: periods of elevated market volatility coincide with higher loadings on the cosine term, while calmer periods correspond to lower values. This pattern reflects the fundamental property of the cosine basis: being even  $(\cos(-x) = \cos(x))$ , it loads exclusively on symmetric features of the return distribution, including dispersion, volatility, and higher-order symmetric shape. Empirically, the strong correlation with the VIX confirms that the cosine coefficient behaves as an endogenous volatility factor in real markets, just as it does in the simulation environment.

The sine coefficient, by contrast, captures distributional asymmetry. Figure 6 compares the average sine coefficients across regions, revealing a clear ordering: the United States exhibits the largest sine coefficient, followed by the Euro area, and then Asian markets. This pattern is consistent with well-documented regional differences in asymmetry, where US markets tend to respond more strongly to negative shocks, European markets show moderate asymmetry, and Asian markets exhibit relatively smaller skew. The sine function's odd form  $(\sin(-x) = -\sin(x))$  ensures that it loads only on asymmetric components of the return distribution, making it a natural proxy for cross-market skewness.

Taken together, the cosine and sine coefficients provide a clean decomposition of market dynamics into symmetric and asymmetric components. This decomposition highlights a key advantage of the Fourier representation: the factors retain stable economic meaning across both simulated and real-world settings because they are tied to pre-specified functional forms rather than sample-specific variation. This robustness contrasts with data-driven approaches such as functional PCA, where the shapes and interpretations of components may shift across samples or time periods.

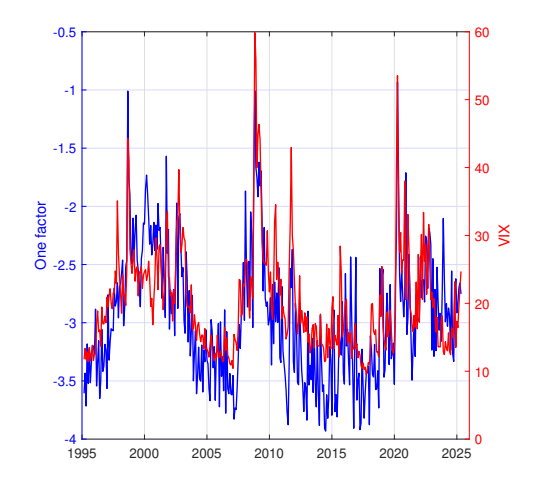


Figure 5: One factor and the VIX index.

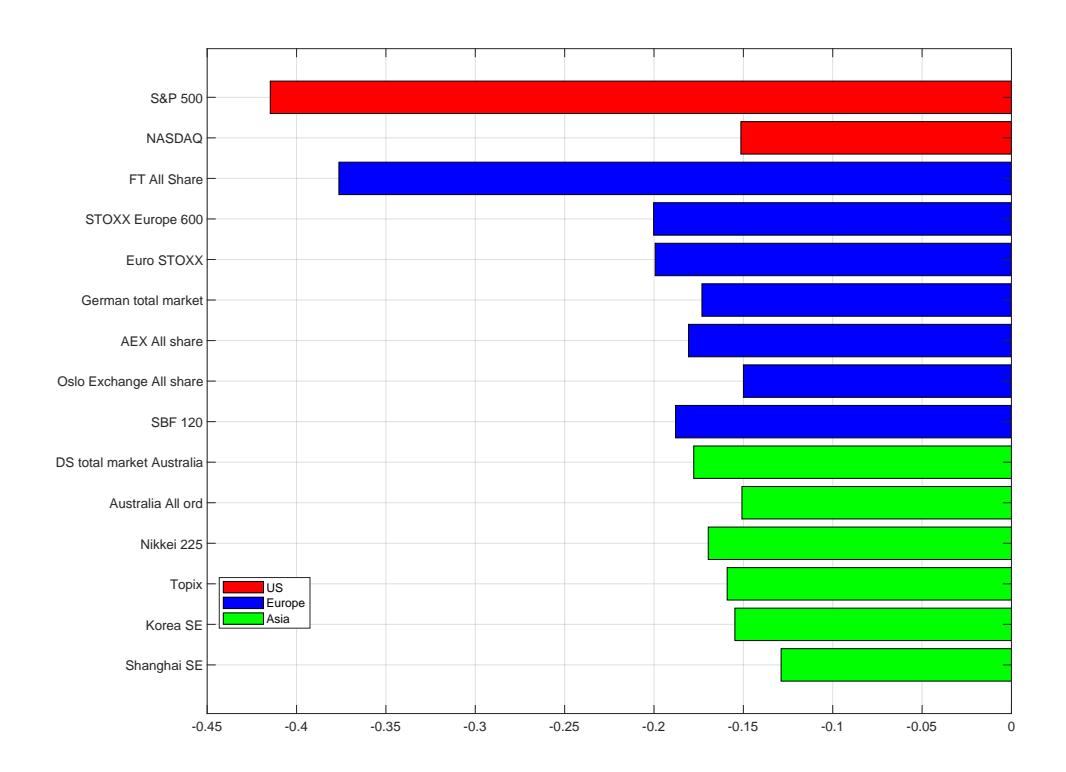


Figure 6: Stock return asymmetry across global markets (average sine component loading).

# D Forecasting Performance Comparison

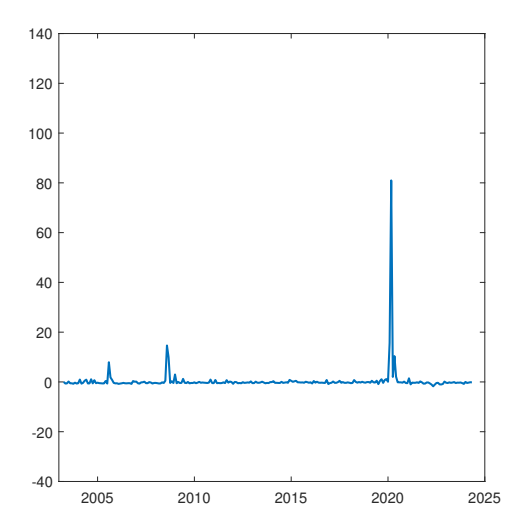
#### D.1 Forecasting macro variables

Table 5 reports the performance of jointly forecasting U.S. macro variable at three horizons using the joint log predictive likelihood. A larger value indicates more accurate density forecast, and the bold figure indicates the best model in each case. The column h=1 can be regarded as an approximation of the marginal likelihood (Geweke, 2001). Two points are immediately clear from these results. First, mvfVAR or sktVAR always provides better fit of data than VAR. Thus, incorporating distributional features, rather than simple overall indices, is beneficial to forecast the macroeconomy. Second, our proposed model, by considering the entire distribution, beats the model which only includes parameters extracted from skew t distributions. Third, considering global stock indices is helpful to improve the forecasting performance compared to focusing solely on the US.

Table 5: Jointly forecasting the three macro variables.

	h = 1	h=2	h = 3
VAR	-17.68	-62.34	-92.46
$\operatorname{sktVAR}$	-4.76	-32.31	-50.25
mvfVAR	9.76	7.17	5.23
mvfVAR (US)	5.90	2.94	0.77

Table 5 only offers the mean of forecasting performance during the whole period. To study the performance over time, we take IP as an example and plot Figure 7. Left panel is the performance of sktVAR against VAR, which is calculated as the difference of density forecast for IP between sktVAR and VAR over time. A positive value means sktVAR outperforms VAR. Right panel is for mvfVAR against VAR. Both sktVAR and mvfVAR perform much better in March 2020, and slightly better in August 2008 and 2005.



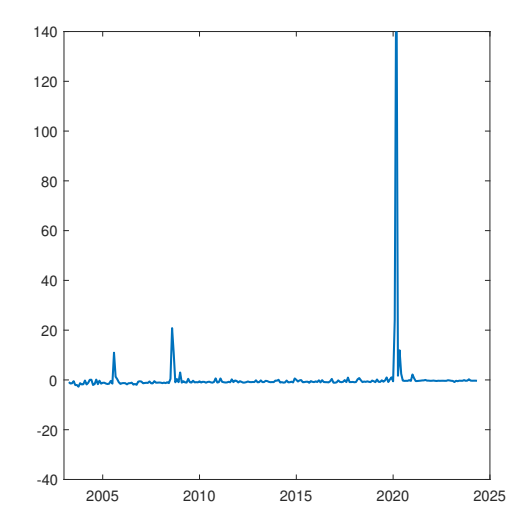


Figure 7: Left panel: sktVAR against VAR (The spike is from March 2020). Right panel: mvfVAR against VAR (Three spikes are from August 2005, August 2008, and March 2020).

The following table reports the forecasting performance for each individual macro variable (both point forecast using RMSFE and density forecast using ALPL). \*, \*\*, \*\*\* denote, respectively, 0.1, 0.05, and 0.01

significance level for a two-sided Diebold and Mariano (2002) test. The benchmark model in the Diebold Mariano test is VAR.

Table 6: Performance of forecasting individual macro variables.

Variables	Models		RMSFE	l I		ALPL	
variables	Models	h=1	h=2	h=3	h=1	h=2	h=3
	VAR	0.01	0.02	0.02	2.41	0.44	-0.87
Industrial Production	$\operatorname{sktVAR}$	0.01	0.02	0.02	2.78	1.64	0.88
muustiai Fioduction	mvfVAR	0.01*	0.02	0.03	2.81	2.17	1.96
	mvfVAR (US)	0.02	0.03	0.03	2.40	1.29	0.77
	VAR	0.01	0.01	0.02	3.26	2.63	2.19
Producer Price Index	$\operatorname{sktVAR}$	0.01	0.02*	0.02	3.18**	2.63*	2.28
1 roducer 1 rice ilidex	mvfVAR	0.01	0.02*	0.03**	2.87**	2.40**	2.11
	mvfVAR (US)	0.01	0.02	0.02	2.92*	2.29**	1.84**
	VAR	0.18	0.32	0.47	0.34	-0.38	-0.88
Federal Funds Rate	$\operatorname{sktVAR}$	0.23*	0.39	0.53	0.11	-0.43	-0.76
rederar runds nate	mvfVAR	0.17	0.32	0.46	0.34	-0.27	-0.68
	mvfVAR (US)	0.14*	0.27	0.40	0.57*	-0.19	-0.71

#### D.2 Forecasting stock market return distributions

To evaluate the predictive accuracy of stock return distributions, we calculate quantile scores. The nine selected quantiles are  $10\%, 20\%, 30\%, \dots, 90\%$ . Our benchmark is the empirical return distribution, which is observed on a monthly basis. The quantile scores from mvfVAR are derived as: i) mvfVAR produces forecasts of log density at evaluation points; ii) forecasts of density is obtained by exponentiating the log density values; iii) compute the cumulative distribution function (cdf) based on evaluation points and forecasts of density;  $^6$  iv) cdf is normalised to ensure it goes from 0 to 1; v) compute quantile scores.  $^7$ 

The quantile scores from sktVAR is obtained in a similar manner, with the key difference being how the density forecasts are generated: sktVAR produces forecasts for the four parameters of the skew t distribution. Consequently, the density forecasts are derived from the skew t distribution. iii) to v) are the same as mvfVAR.

Since the forecast of quantile score is a point forecast, RMSFE can be used to compare different models. However, reporting the results is challenging, as there are 15 indices, each with 9 quantile score forecasts, leading to a total of 135 point forecasts. To address this, we conducted comparisons in various ways and observed consistent patterns for each quantile score across the indices. As a result, we averaged the RMSFE for each quantile score across all indices, which provides sharper insights based on the nine quantile score forecasts. The averaged RMSFE is reported in Table 7. Q1 is for quantile 10%, and Q9 is for quantile 90%.

When forecasting the middle quantile scores (Q3, Q4, Q5, Q6, Q7), the differences between the two approaches are minimal. However, for the upper quantile scores (Q8, Q9) and particularly the lower quantile scores (Q1, Q2), the differences become more pronounced, with mvfVAR consistently outperforming sktVAR.

<sup>&</sup>lt;sup>6</sup>This is done using Matlab function *cumtrapz*.

<sup>&</sup>lt;sup>7</sup>This is done by using Matlab function interp1. 'method' is set to 'linear'. 'extrapolation' is set to 'extrap'.

Table 7: The Average	d RMSFE of nin	e quantile scores.
----------------------	----------------	--------------------

		Q1	Q2	Q3	Q4	Q5	Q6	Q7	Q8	Q9
h=1	sktVAR mvfVAR	0.132	0.093	0.072	0.059	0.052	0.052	0.06	0.079	0.117
n-1	mvfVAR	0.085	0.07	0.064	0.06	0.057	0.056	0.056	0.06	0.074
h=2	sktVAR	0.132	0.093	0.072	0.059	0.052	0.052	0.06	0.078	0.117
n = 2	$\operatorname{mvfVAR}$	0.086	0.072	0.064	0.06	0.057	0.055	0.055	0.059	0.074
h=3	sktVAR	0.132	0.093	0.072	0.058	0.052	0.052	0.06	0.078	0.117
n = 3	$\operatorname{mvfVAR}$	0.083	0.069	0.062	0.058	0.056	0.055	0.055	0.059	0.074

# E Impulse response functions

In this section, we first report the IRFs for the macro, followed by the distributional IRFs for longer horizons.

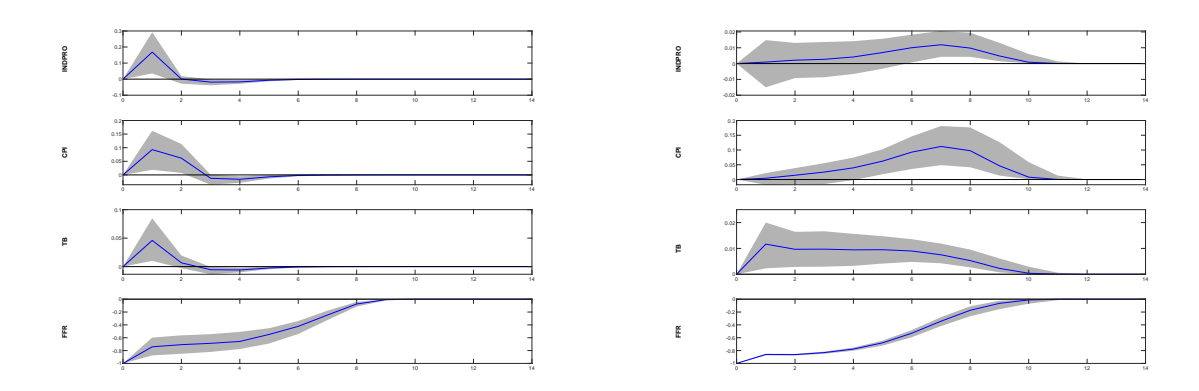


Figure 8: IRFs for the macro variables over horizons. Left: skew-t VAR; Right: mvfVAR which is based on Fourier basis functions. The monetary policy shock occurs at h=0 which decreases the policy rate by 1 percent. The instrument of policy rate is the Federal funds rate and it enters the VAR in percent.

Next, we report the distributional IRFs. Section 3 has reported the change in the four moments from mvfVAR at h = 0. Here we report longer horizons from mvfVAR.

Table 8: Changes in the four moments of return distributions at horizon h = 1 (from mvfVAR model).

	Mean		Volatility		Skewness	· · · · · · · · · · · · · · · · · · ·	Kurtosis	
	Expansionary	Contractionary	Expansionary	Contractionary	Expansionary	Contractionary	Expansionary	Contractionary
S&P 500	-0.01	0.01	0	0	0.01	-0.01	0.08	-0.07
	(-0.01, -0.00)	(0.00, 0.01)	(-0.01, -0.00)	(0.00, 0.01)	(0.00, 0.03)	(-0.03, -0.00)	(0.02, 0.18)	(-0.15, -0.02)
NASDAQ	0	0	0.04	-0.04	0	0	-0.01	0.01
	(-0.00, -0.00)	(0.00, 0.00)	(0.01, 0.09)	(-0.10, -0.01)	(0.00, 0.00)	(-0.00, -0.00)	(-0.02, -0.00)	(0.00, 0.02)
FT All Share	0	0	0.36	-0.36	0	0	-0.35	0.38
	(-0.00, -0.00)	(0.00, 0.00)	(0.11, 0.76)	(-0.73, -0.11)	(-0.00, -0.00)	(0.00, 0.00)	(-0.70, -0.11)	(0.11, 0.82)
Europe 600	0	0	-0.24	0.24	0.01	0	0.13	-0.13
	(-0.01, -0.00)	(0.00, 0.01)	(-0.51, -0.07)	(0.07, 0.51)	(0.00, 0.01)	(-0.01, -0.00)	(0.04, 0.28)	(-0.26, -0.04)
EURO STOXX	0	0	-0.25	0.25	0.01	0	0.13	-0.13
	(-0.01, -0.00)	(0.00, 0.01)	(-0.51, -0.07)	(0.07, 0.52)	(0.00, 0.01)	(-0.01, -0.00)	(0.04, 0.28)	(-0.26, -0.04)
German	0	0	-0.27	0.27	0	0	0.09	-0.09
	(-0.01, -0.00)	(0.00, 0.01)	(-0.56, -0.08)	(0.08, 0.56)	(0.00, 0.01)	(-0.01, -0.00)	(0.03, 0.20)	(-0.18, -0.03)
AEX All Share	0	0	-0.27	0.27	0	0	0.11	-0.11
	(-0.01, -0.00)	(0.00, 0.01)	(-0.57, -0.08)	(0.08, 0.57)	(0.00, 0.01)	(-0.01, -0.00)	(0.03, 0.23)	(-0.21, -0.03)
Oslo	0	0	-0.26	0.26	0	0	0.07	-0.07
	(-0.00, -0.00)	(0.00, 0.00)	(-0.55, -0.07)	(0.07, 0.55)	(0.00, 0.00)	(-0.00, -0.00)	(0.02, 0.15)	(-0.14, -0.02)
SBF 120	0	0	-0.26	0.26	0	0	0.11	-0.11
	(-0.01, -0.00)	(0.00, 0.01)	(-0.54, -0.07)	(0.07, 0.54)	(0.00, 0.01)	(-0.01, -0.00)	(0.03, 0.24)	(-0.22, -0.03)
DS Australia	0	0	-0.28	0.28	0	0	0.1	-0.1
	(-0.01, -0.00)	(0.00, 0.01)	(-0.57, -0.08)	(0.08, 0.57)	(0.00, 0.01)	(-0.01, -0.00)	(0.03, 0.22)	(-0.20, -0.03)
Australia	0	0	-0.26	0.26	0	0	0.07	-0.07
	(-0.01, -0.00)	(0.00, 0.00)	(-0.55, -0.07)	(0.07, 0.55)	(0.00, 0.00)	(-0.00, -0.00)	(0.02, 0.15)	(-0.14, -0.02)
Nikkei	0	0	-0.29	0.29	0	0	0.1	-0.1
	(-0.01, -0.00)	(0.00, 0.01)	(-0.61, -0.08)	(0.08, 0.61)	(0.00, 0.01)	(-0.01, -0.00)	(0.03, 0.21)	(-0.19, -0.03)
Topix	0	0	-0.3	0.3	0	0	0.09	-0.09
	(-0.01, -0.00)	(0.00, 0.01)	(-0.62, -0.08)	(0.08, 0.62)	(0.00, 0.01)	(-0.01, -0.00)	(0.03, 0.19)	(-0.18, -0.02)
Korea	0	0	-0.29	0.28	0	0	0.08	-0.07
	(-0.01, -0.00)	(0.00, 0.01)	(-0.60, -0.08)	(0.08, 0.59)	(0.00, 0.01)	(-0.01, -0.00)	(0.02, 0.16)	(-0.15, -0.02)
SHANGHAI SE	0	0	-0.33	0.33	0	0	0.07	-0.07
	(-0.01, -0.00)	(0.00, 0.01)	(-0.70, -0.10)	(0.09, 0.69)	(0.00, 0.00)	(-0.00, -0.00)	(0.02, 0.15)	(-0.13, -0.02)

Values in the brackect are the 16% and 84% confidence intervals. In order to optimize space utilization, a series of abbreviations were employed, each representing: Europe 600 for STOXX Europe 600, German for German total market, Oslo for Oslo Exchange All Share, DS Australia for DS total market Australia, Australia for Australia All ordinaries, Nikkei for Nikkei 225 Stock, Korea for Korea Stock Exchange.

Table 9: Changes in the four moments of return distributions at horizon h = 9 (from mvfVAR model).

	Mean		Volatility		Skewness		Kurtosis	
	Expansionary	Contractionary	Expansionary	Contractionary	Expansionary	Contractionary	Expansionary	Contractionar
S&P 500	-0.02	0.02	0	0	0.02	-0.04	-0.07	0.08
	(-0.03, -0.01)	(0.01, 0.03)	(0.00, 0.01)	(-0.01, -0.00)	(-0.01, 0.05)	(-0.07, -0.01)	(-0.14, -0.03)	(0.03, 0.19)
NASDAQ	-0.01	0.01	0.01	-0.01	0.01	-0.01	0	0
	(-0.02, 0.00)	(-0.00, 0.02)	(0.00, 0.03)	(-0.03, -0.00)	(0.00, 0.02)	(-0.02, -0.00)	(-0.01, -0.00)	(0.00, 0.01)
FT All Share	-0.03	0.03	-0.01	0.01	0.04	-0.03	0.01	-0.01
	(-0.04, -0.02)	(0.02, 0.04)	(-0.02, 0.00)	(-0.01, 0.02)	(0.02, 0.06)	(-0.04, -0.02)	(-0.00, 0.03)	(-0.02, 0.01)
Europe 600	0.01	ò	0.03	-0.02	-0.02	0.02	-0.01	0.02
-	(0.00, 0.02)	(-0.01, 0.00)	(0.01, 0.05)	(-0.04, -0.01)	(-0.03, -0.01)	(0.01, 0.03)	(-0.02, -0.01)	(0.01, 0.03)
EURO STOXX	0.01	ò	0.03	-0.02	-0.02	0.02	-0.01	0.02
	(0.00, 0.02)	(-0.01, 0.00)	(0.01, 0.05)	(-0.04, -0.01)	(-0.03, -0.01)	(0.01, 0.03)	(-0.02, -0.01)	(0.01, 0.03)
German	0.01	ò	0.03	-0.03	-0.01	0.01	-0.01	0.01
	(0.00, 0.01)	(-0.01, 0.00)	(0.02, 0.05)	(-0.04, -0.01)	(-0.02, -0.00)	(0.00, 0.02)	(-0.01, -0.00)	(0.01, 0.02)
AEX All Share	0.01	-0.01	0.03	-0.03	-0.01	0.01	-0.01	0.01
	(0.00, 0.02)	(-0.01, 0.00)	(0.02, 0.05)	(-0.04, -0.01)	(-0.02, -0.01)	(0.01, 0.03)	(-0.01, -0.01)	(0.01, 0.02)
Oslo	Ô	0	0.03	-0.03	0	Ô	-0.01	0.01
	(-0.00, 0.00)	(-0.00, 0.01)	(0.02, 0.05)	(-0.04, -0.02)	(-0.00, 0.00)	(-0.00, 0.00)	(-0.01, -0.00)	(0.00, 0.02)
SBF 120	0.01	0	0.03	-0.02	-0.01	0.01	-0.01	0.01
	(0.00, 0.02)	(-0.01, 0.00)	(0.01, 0.05)	(-0.04, -0.01)	(-0.02, -0.01)	(0.01, 0.03)	(-0.01, -0.01)	(0.01, 0.02)
OS Australia	0.01	-0.01	0.03	-0.03	-0.01	0.01	-0.01	0.01
	(0.00, 0.02)	(-0.01, 0.00)	(0.02, 0.05)	(-0.04, -0.01)	(-0.02, -0.01)	(0.01, 0.03)	(-0.01, -0.01)	(0.01, 0.02)
Australia	Ô	0	0.03	-0.03	0	Ô	-0.01	0.01
	(-0.00, 0.01)	(-0.01, 0.00)	(0.02, 0.05)	(-0.04, -0.02)	(-0.01, 0.00)	(-0.00, 0.01)	(-0.01, -0.00)	(0.00, 0.02)
Nikkei	0.01	-0.01	0.03	-0.03	-0.01	0.01	-0.01	0.01
	(0.00, 0.02)	(-0.01, -0.00)	(0.02, 0.05)	(-0.04, -0.02)	(-0.02, -0.01)	(0.01, 0.03)	(-0.01, -0.00)	(0.01, 0.02)
Горіх	0.01	ò	0.03	-0.03	-0.01	0.01	-0.01	0.01
•	(0.00, 0.01)	(-0.01, 0.00)	(0.02, 0.05)	(-0.04, -0.02)	(-0.01, -0.00)	(0.00, 0.02)	(-0.01, -0.00)	(0.01, 0.02)
Corea	0.01	Ò	0.03	-0.03	-0.01	0.01	-0.01	0.01
	(0.00, 0.01)	(-0.01, 0.00)	(0.02, 0.04)	(-0.04, -0.02)	(-0.01, -0.00)	(0.00, 0.02)	(-0.01, -0.00)	(0.00, 0.02)
SHANGHAI SE	0	Ò	0.03	-0.03	-0.01	0.01	-0.01	0.01
	(0.00, 0.01)	(-0.01, -0.00)	(0.02, 0.05)	(-0.05, -0.02)	(-0.01, -0.00)	(0.00, 0.01)	(-0.01, -0.00)	(0.00, 0.01)

Values in the bracket are the 16% and 84% confidence intervals. In order to optimize space utilization, a series of abbreviations were employed, each representing: Europe 600 for STOXX Europe 600, German for German total market, Oslo for Oslo Exchange All Share, DS Australia for DS total market Australia, Australia for Australia All ordinaries, Nikkei for Nikkei 225 Stock, Korea for Korea Stock Exchange.

To conclude this section, we report the change in the four moments from sktVAR across the three horizons.

Table 10: Changes in the four moments of return distributions at horizon h = 0 (from sktVAR).

	Mean	· · · · · · · · · · · · · · · · · · ·	Volatility		Skewness	· · · · · · · · · · · · · · · · · · ·	Kurtosis	
	Expansionary	Contractionary	Expansionary	Contractionary	Expansionary	Contractionary	Expansionary	Contractionary
S&P 500	0.08	-0.08	-0.44	1.07	0.3	-0.3	-1.21	2.28
	(-0.44, 0.63)	(-0.63, 0.44)	(-0.52, -0.31)	(0.54, 1.68)	(-0.14, 0.83)	(-0.83, 0.14)	(-1.50, -0.83)	(1.22, 3.59)
NASDAQ	0.13	-0.13	-0.27	0.34	0.02	-0.02	-0.35	0.42
	(-0.12, 0.44)	(-0.44, 0.12)	(-0.35, -0.17)	(0.20, 0.48)	(-0.18, 0.21)	(-0.21, 0.18)	(-0.48, -0.24)	(0.27, 0.61)
FT All Share	0.04	-0.04	-0.31	0.53	0.24	-0.24	-0.7	0.97
	(-0.11, 0.20)	(-0.20, 0.11)	(-0.38, -0.20)	(0.27, 0.78)	(0.12, 0.36)	(-0.36, -0.12)	(-0.91, -0.41)	(0.49, 1.42)
Europe 600	0.06	-0.06	-0.38	0.61	0.22	-0.22	-0.61	0.75
	(-0.17, 0.33)	(-0.33, 0.17)	(-0.48, -0.24)	(0.32, 0.94)	(0.08, 0.42)	(-0.42, -0.08)	(-0.86, -0.35)	(0.39, 1.19)
EURO STOXX	0.07	-0.07	-0.32	0.51	0.31	-0.31	-0.41	0.48
	(-0.18, 0.36)	(-0.36, 0.18)	(-0.42, -0.21)	(0.29, 0.81)	(0.10, 0.54)	(-0.54, -0.10)	(-0.62, -0.16)	(0.17, 0.78)
German	0.07	-0.07	-0.23	0.32	0.36	-0.36	-0.43	0.51
	(-0.15, 0.31)	(-0.31, 0.15)	(-0.31, -0.14)	(0.16, 0.49)	(0.13, 0.58)	(-0.58, -0.13)	(-0.67, -0.22)	(0.24, 0.92)
AEX All Share	0.07	-0.07	-0.26	0.39	0.16	-0.16	-0.68	0.96
	(-0.12, 0.25)	(-0.25, 0.12)	(-0.33, -0.16)	(0.21, 0.59)	(-0.03, 0.32)	(-0.32, 0.03)	(-0.96, -0.44)	(0.54, 1.65)
Oslo	0.02	-0.02	-0.12	0.14	0.18	-0.18	-0.38	0.46
	(-0.13, 0.17)	(-0.17, 0.13)	(-0.19, -0.06)	(0.06, 0.24)	(0.01, 0.37)	(-0.37, -0.01)	(-0.57, -0.19)	(0.21, 0.75)
SBF 120	0.08	-0.08	-0.41	0.63	0.14	-0.14	-0.39	0.44
	(-0.18, 0.38)	(-0.38, 0.18)	(-0.53, -0.27)	(0.35, 0.98)	(-0.08, 0.50)	(-0.50, 0.08)	(-0.66, -0.10)	(0.11, 0.82)
DS Australia	0.07	-0.07	-0.19	0.24	0.12	-0.12	-0.51	0.64
	(-0.12, 0.27)	(-0.27, 0.12)	(-0.25, -0.09)	(0.10, 0.35)	(-0.03, 0.25)	(-0.25, 0.03)	(-0.80, -0.22)	(0.25, 1.15)
Australia	0.06	-0.06	-0.06	0.06	0.03	-0.03	-0.2	0.22
	(-0.10, 0.23)	(-0.23, 0.10)	(-0.10, -0.02)	(0.02, 0.11)	(-0.06, 0.11)	(-0.11, 0.06)	(-0.34, -0.06)	(0.06, 0.40)
Nikkei	0.1	-0.1	-0.23	0.31	0.61	-0.61	-0.16	0.16
	(-0.13, 0.31)	(-0.31, 0.13)	(-0.30, -0.13)	(0.15, 0.44)	(0.26, 0.89)	(-0.89, -0.26)	(-0.30, 0.09)	(-0.08, 0.33)
Topix	0.04	-0.04	-0.15	0.18	0.51	-0.51	-0.34	0.39
	(-0.05, 0.14)	(-0.14, 0.05)	(-0.19, -0.08)	(0.10, 0.26)	(0.32, 0.77)	(-0.77, -0.32)	(-0.49, -0.20)	(0.22, 0.60)
Korea	0.05	-0.05	-0.12	0.14	0.26	-0.26	-0.16	0.17
	(-0.04, 0.14)	(-0.14, 0.04)	(-0.17, -0.07)	(0.07, 0.21)	(0.13, 0.38)	(-0.38, -0.13)	(-0.25, -0.04)	(0.04, 0.28)
SHANGHAI SE	0.04	-0.04	0	0	0.53	-0.53	-0.32	0.37
	(-0.07, 0.15)	(-0.15, 0.07)	(-0.03, 0.03)	(-0.02, 0.03)	(0.30, 0.83)	(-0.83, -0.30)	(-0.53, -0.17)	(0.18, 0.67)

Values in the bracket are the 16% and 84% confidence intervals. In order to optimize space utilization, a series of abbreviations were employed, each representing: Europe 600 for STOXX Europe 600, German for German total market, Oslo for Oslo Exchange All Share, DS Australia for DS total market Australia, Australia for Australia All ordinaries, Nikkei for Nikkei 225 Stock, Korea for Korea Stock Exchange.

Table 11: Changes in the four moments of return distributions at horizon h = 1 (from sktVAR).

	Mean		Volatility		Skewness		Kurtosis	
	Expansionary	Contractionary	Expansionary	Contractionary	Expansionary	Contractionary	Expansionary	Contractionary
S&P 500	0.07	-0.07	-0.03	0.04	-0.05	0.05	0.02	-0.02
	(0.02, 0.13)	(-0.13, -0.02)	(-0.07, 0.00)	(-0.00, 0.08)	(-0.11, 0.00)	(-0.00, 0.11)	(-0.12, 0.15)	(-0.14, 0.13)
NASDAQ	0.08	-0.08	-0.07	0.07	-0.11	0.11	-0.11	0.11
	(0.02, 0.14)	(-0.14, -0.02)	(-0.13, -0.02)	(0.02, 0.14)	(-0.17, -0.03)	(0.03, 0.17)	(-0.23, -0.01)	(0.01, 0.26)
FT All Share	0.08	-0.08	-0.07	0.08	-0.11	0.11	-0.08	0.08
	(0.02, 0.13)	(-0.13, -0.02)	(-0.11, -0.04)	(0.04, 0.13)	(-0.17, -0.05)	(0.05, 0.17)	(-0.27, 0.08)	(-0.08, 0.31)
Europe 600	0.05	-0.05	-0.06	0.07	-0.08	0.08	0.23	-0.22
-	(0.01, 0.10)	(-0.10, -0.01)	(-0.09, -0.02)	(0.02, 0.10)	(-0.14, -0.02)	(0.02, 0.14)	(-0.02, 0.43)	(-0.38, 0.02)
EURO STOXX	0.05	-0.05	-0.1	0.11	-0.1	0.1	0.07	-0.07
	(0.00, 0.10)	(-0.10, -0.00)	(-0.14, -0.05)	(0.05, 0.17)	(-0.21, -0.03)	(0.03, 0.21)	(-0.10, 0.26)	(-0.24, 0.11)
German	0.09	-0.09	-0.05	0.05	-0.15	0.15	-0.16	0.17
	(0.02, 0.16)	(-0.16, -0.02)	(-0.09, -0.02)	(0.02, 0.10)	(-0.25, -0.06)	(0.06, 0.25)	(-0.35, 0.00)	(-0.00, 0.40)
AEX All Share	0.06	-0.06	-0.09	0.1	-0.06	0.06	0.12	-0.11
	(0.01, 0.10)	(-0.10, -0.01)	(-0.13, -0.04)	(0.05, 0.16)	(-0.12, -0.01)	(0.01, 0.12)	(0.02, 0.30)	(-0.27, -0.02)
Oslo	0.05	-0.05	-0.09	0.1	0	Ô	0.28	-0.25
	(0.01, 0.10)	(-0.10, -0.01)	(-0.13, -0.05)	(0.05, 0.15)	(-0.03, 0.03)	(-0.03, 0.03)	(0.11, 0.46)	(-0.38, -0.10)
SBF 120	0.06	-0.06	-0.19	0.23	-0.13	0.13	-0.45	0.52
	(0.01, 0.13)	(-0.13, -0.01)	(-0.27, -0.12)	(0.13, 0.35)	(-0.23, -0.06)	(0.06, 0.23)	(-0.65, -0.26)	(0.28, 0.80)
DS Australia	0.03	-0.03	-0.13	0.15	-0.05	0.05	-0.13	0.13
	(0.01, 0.05)	(-0.05, -0.01)	(-0.17, -0.06)	(0.07, 0.22)	(-0.11, -0.01)	(0.01, 0.11)	(-0.29, -0.01)	(0.01, 0.33)
Australia	0.04	-0.04	-0.08	0.09	0.01	-0.01	0.09	-0.08
	(-0.02, 0.09)	(-0.09, 0.02)	(-0.11, -0.04)	(0.04, 0.13)	(-0.02, 0.07)	(-0.07, 0.02)	(-0.08, 0.23)	(-0.21, 0.08)
Nikkei	-0.02	0.02	-0.11	0.13	0.03	-0.03	-0.24	0.26
	(-0.05, 0.00)	(-0.00, 0.05)	(-0.16, -0.06)	(0.06, 0.19)	(-0.02, 0.11)	(-0.11, 0.02)	(-0.47, -0.07)	(0.07, 0.55)
Горіх	-0.01	0.01	-0.12	0.15	0.13	-0.13	-0.21	0.23
•	(-0.03, 0.01)	(-0.01, 0.03)	(-0.18, -0.05)	(0.05, 0.25)	(0.06, 0.22)	(-0.22, -0.06)	(-0.37, -0.06)	(0.06, 0.43)
Korea	0.03	-0.03	-0.09	0.1	0.24	-0.24	-0.04	0.04
	(-0.02, 0.08)	(-0.08, 0.02)	(-0.14, -0.04)	(0.04, 0.17)	(0.13, 0.35)	(-0.35, -0.13)	(-0.10, 0.02)	(-0.02, 0.10)
SHANGHAI SE	ò	Ò	-0.04	0.04	0.12	-0.12	-0.08	0.08
	(-0.07, 0.05)	(-0.05, 0.07)	(-0.06, -0.01)	(0.01, 0.07)	(0.03, 0.22)	(-0.22, -0.03)	(-0.52, 0.42)	(-0.36, 0.65)

Values in the brackeet are the 16% and 84% confidence intervals. In order to optimize space utilization, a series of abbreviations were employed, each representing: Europe 600 for STOXX Europe 600, German for German total market, Oslo for Oslo Exchange All Share, DS Australia for DS total market Australia, Australia for Australia All ordinaries, Nikkei for Nikkei 225 Stock, Korea for Korea Stock Exchange.

Table 12: Changes	in the four moments of	return distributions at	horizon $h = 9$	(from sktVAR).

	Mean		Volatility		Skewness		Kurtosis	
	Expansionary	Contractionary	Expansionary	Contractionary	Expansionary	Contractionary	Expansionary	Contractionary
S&P 500	0	0	0	0	0	0	0	0
	(-0.00, 0.00)	(-0.00, 0.00)	(0.00, 0.00)	(-0.00, -0.00)	(-0.00, -0.00)	(0.00, 0.00)	(0.00, 0.00)	(-0.00, -0.00)
NASDAQ	0	0	0	0	0	0	0	0
	(-0.00, 0.00)	(-0.00, 0.00)	(0.00, 0.00)	(-0.00, -0.00)	(-0.00, -0.00)	(0.00, 0.00)	(0.00, 0.00)	(-0.00, -0.00)
FT All Share	0	0	0	0	0	0	0	0
	(-0.00, 0.00)	(-0.00, 0.00)	(0.00, 0.00)	(-0.00, -0.00)	(-0.00, -0.00)	(0.00, 0.00)	(0.00, 0.00)	(-0.00, -0.00)
Europe 600	0	0	0	0	0	0	0	0
	(-0.00, 0.00)	(-0.00, 0.00)	(0.00, 0.00)	(-0.00, -0.00)	(-0.00, -0.00)	(0.00, 0.00)	(0.00, 0.00)	(-0.00, -0.00)
EURO STOXX	0	0	0	0	0	0	0	0
	(-0.00, 0.00)	(-0.00, 0.00)	(0.00, 0.00)	(-0.00, -0.00)	(-0.00, -0.00)	(0.00, 0.00)	(0.00, 0.00)	(-0.00, -0.00)
German	0	0	0	0	0	0	0	0
	(-0.00, 0.00)	(-0.00, 0.00)	(0.00, 0.00)	(-0.00, -0.00)	(-0.00, 0.00)	(-0.00, 0.00)	(0.00, 0.00)	(-0.00, -0.00)
AEX All Share 0	0	0	0	0	0	0	0	0
	(-0.00, 0.00)	(-0.00, 0.00)	(0.00, 0.00)	(-0.00, -0.00)	(-0.00, -0.00)	(0.00, 0.00)	(0.00, 0.00)	(-0.00, -0.00)
Oslo	0	0	0	0	0	0	0	0
	(-0.00, 0.00)	(-0.00, 0.00)	(0.00, 0.00)	(-0.00, -0.00)	(-0.00, -0.00)	(0.00, 0.00)	(0.00, 0.00)	(-0.00, -0.00)
SBF 120	0	0	0	0	0	0	0	0
	(-0.00, 0.00)	(-0.00, 0.00)	(0.00, 0.00)	(-0.00, -0.00)	(-0.00, -0.00)	(0.00, 0.00)	(-0.00, 0.00)	(-0.00, 0.00)
DS Australia	0	0	0	0	0	0	0	0
	(-0.00, 0.00)	(-0.00, 0.00)	(0.00, 0.00)	(-0.00, -0.00)	(-0.00, -0.00)	(0.00, 0.00)	(0.00, 0.00)	(-0.00, -0.00)
Australia	0	0	0	0	0	0	0	0
	(-0.00, 0.00)	(-0.00, 0.00)	(0.00, 0.00)	(-0.00, -0.00)	(-0.00, -0.00)	(0.00, 0.00)	(0.00, 0.00)	(-0.00, -0.00)
Nikkei	0	0	0	0	0	0	0	0
	(-0.00, 0.00)	(-0.00, 0.00)	(-0.00, 0.00)	(-0.00, 0.00)	(-0.00, -0.00)	(0.00, 0.00)	(0.00, 0.00)	(-0.00, -0.00)
Topix	0	0	0	0	0	0	0	0
	(0.00, 0.00)	(-0.00, -0.00)	(-0.00, -0.00)	(0.00, 0.00)	(0.00, 0.00)	(-0.00, -0.00)	(-0.00, -0.00)	(0.00, 0.00)
Korea	0	0	0	0	0	0	0	0
	(0.00, 0.00)	(-0.00, -0.00)	(-0.00, 0.00)	(-0.00, 0.00)	(0.00, 0.00)	(-0.00, -0.00)	(-0.00, -0.00)	(0.00, 0.00)
SHANGHAI SE	0	0	0	0	0	0	0	0
	(0.00, 0.00)	(-0.00, -0.00)	(-0.00, -0.00)	(0.00, 0.00)	(0.00, 0.00)	(-0.00, -0.00)	(-0.00, 0.00)	(-0.00, 0.00)

Values in the bracket are the 16% and 84% confidence intervals. In order to optimize space utilization, a series of abbreviations were employed, each representing: Europe 600 for STOXX Europe 600, German for German total market, Oslo for Oslo Exchange All Share, DS Australia for DS total market Australia, Australia for Australia All ordinaries, Nikkei for Nikkei 225 Stock, Korea for Korea Stock Exchange.

# F Implementation details

#### F.1 Fourier basis functions

The return data is truncated at 0.5% (Lower Bound, LB) and 99.5% (Upper Bound, UB) percentiles and we rescale them to the interval [0, 1] by taking the cumulative distribution function of the standard normal distribution ( $y_i^{\text{scaled}}$ ). The design matrix  $\Phi$  ( $\mathbf{y}$ ) is then constructed as follows:

$$\boldsymbol{\Phi}\left(\mathbf{y}\right) = \begin{bmatrix} \sin(2\pi y_{1}^{\text{scaled}}) & \cos(2\pi y_{1}^{\text{scaled}}) & \sin(4\pi y_{1}^{\text{scaled}}) & \cos(4\pi y_{1}^{\text{scaled}}) \\ \sin(2\pi y_{2}^{\text{scaled}}) & \cos(2\pi y_{2}^{\text{scaled}}) & \sin(4\pi y_{2}^{\text{scaled}}) & \cos(4\pi y_{2}^{\text{scaled}}) \\ & \dots & \dots & \dots & \dots \\ \sin(2\pi y_{n-1}^{\text{scaled}}) & \cos(2\pi y_{n-1}^{\text{scaled}}) & \sin(4\pi y_{n-1}^{\text{scaled}}) & \cos(4\pi y_{n-1}^{\text{scaled}}) \\ \sin(2\pi y_{n}^{\text{scaled}}) & \cos(2\pi y_{n}^{\text{scaled}}) & \sin(4\pi y_{n}^{\text{scaled}}) & \cos(4\pi y_{n}^{\text{scaled}}) \\ \end{bmatrix}.$$

This matrix captures the Fourier basis functions evaluated at the rescaled points  $y_i^{\text{scaled}}$ . For simplicity, we will omit the superscript scaled in the following.

## F.2 Bayesian inference

The resulting functional VAR resembles a factor-augmented VAR

$$X_{t} = b + \sum_{p=1}^{P} B_{p} X_{t-p} + \epsilon_{t}, \quad \epsilon_{t} \sim N\left(\mathbf{0}_{dim}, \Sigma\right)$$

where  $X_t = [vec(\mathbf{Z}_t)', z_t']'$  and  $z_t$  denotes the macro variables. Therefore, standard Bayesian estimation for the VAR can be used here. The prior for VAR coefficients  $B_p$  follows Chan (2022). We start with a VAR(p) in structural form,

$$A_0 X_t = a + \sum_{p=1}^{P} A_p X_{t-p} + \epsilon_t, \quad \epsilon_t \sim N\left(\mathbf{0}_{dim}, \Lambda\right),$$

where  $A_0$  is a lower triangular matrix with ones on its main diagonal and  $\Lambda = \text{diag}(\sigma_1^2, \sigma_2^2, \dots, \sigma_{dim}^2)$ . This allows us to estimate the VAR equation by equation. The *i*-th equation can be written as

$$x_{it} = w_{it}\alpha_i + z_{it}\theta_i + \varepsilon_{it}, \quad \epsilon_t \sim N\left(0, \sigma_i^2\right),$$

where  $w_{it} = (-y_{1t}, -y_{2t}, \dots, -y_{i-1t})$  and  $z_{it} = (1, X'_{t-1}, \dots, X'_{t-p})$ . We use the normal-inverse-gamma prior

$$\alpha_i \mid \sigma_i^2 \sim \mathcal{N}(0, \sigma_i^2 \mathbf{V}_i^\alpha),$$

$$\theta_i \mid \sigma_i^2 \sim \mathcal{N}(0, \sigma_i^2 V_i^\theta),$$

$$\sigma_i^2 \sim \mathcal{IG}(\frac{v_0 + i - n}{2}, \frac{s_i^2}{2}).$$

 $s_i^2$  denotes the sample variance of the residuals from an AR(p) model estimated on variable i. This one is direct to compute for macro variables  $z_t$  as they are observed.

We set  $V_i^{\alpha} = \text{diag}(1/s_i^2, \dots, 1/s_{i-1}^2)$ . For the VAR coefficients  $\theta_i$ , the prior covariance matrix depends on  $V_i^{\theta}$ . It contains three hyperparameters, namely,  $\kappa_1, \kappa_2, \kappa_3$ , that control the degree of shrinkage for different types of coefficients.

$$\mathbf{V}_{i}^{\theta} = \begin{cases} \frac{\kappa_{1}}{l^{2}s_{i}^{2}} & \text{for the coefficient on the $l$th lag of variable $i$} \\ \frac{\kappa_{2}}{l^{2}s_{i}^{2}} & \text{for the coefficient on the $l$th lag of variable $j$} \\ \kappa_{3} & \text{for the intercept} \end{cases}$$

We set  $\kappa_1 = 0.1$ ,  $\kappa_2 = 0.01$ , and  $\kappa_3 = 10$ . For the sktVAR, since the dimension is much higher, we set  $\kappa_1 = 0.01$ ,  $\kappa_2 = 0.001$ . These values suggest that the coefficients associated with lags of other variables undergo greater shrinkage compared to those of their own lags, while the intercepts experience virtually no shrinkage.